3D Printing of Polymer-Particle Composite Using Electrostatic Deposition and In-Situ Photopolymerization

BY

ABHISHEK PATIL
B.E. Mechanical Engineering
Symbiosis International University, Pune, India, 2014

THESIS

Submitted as partial fulfillment of the requirements
for the degree of Master of Science in Industrial Engineering
in the Graduate College of the
University of Illinois at Chicago, 2016

Chicago, Illinois

Defense Committee:

Dr. Yayue Pan, Chair and Advisor
Dr. Lin Li, Mechanical and Industrial Engineering
Dr. Alan Feinerman, Electrical and Computer Engineering

This thesis is dedicated to my parents, Vikas Patil and Neeta Patil, for their unconditional love, support and motivation through all walks of my life.

ACKNOWLEDGEMENT

I would like to thank my advisor, Dr. Yayue Pan, Assistant Professor in the Department of Mechanical and Industrial Engineering at The University of Illinois at Chicago, for giving me an opportunity to work in the laboratory. Also, I want to thank her for guidance, motivation and support throughout the duration of my graduate studies. Her expertise, technical, and editorial advice has been essential to my success as a graduate student and completion of my thesis.

Additionally, I would also like to convey gratitude to Dr. Lin Li and Dr. Alan Feinerman for serving on my graduate committee. Their time, guidance and suggestions in the revision of this thesis are deeply appreciated.

Also, I would also like to thank Dr. Chi Zhou from University at Buffalo, Dr. Ping Guo from The Chinese University of Hong Kong and all my colleagues at the Laboratory of Additive Manufacturing, Education and Research (LAMRE), for their contribution, collaboration and support throughout my research work.

CONTRIBUTION OF AUTHORS

Chapter 1 is an introduction to the background and literature review of multi-material 3D printing technologies, motivation for the research presented herein and scope of the research work. Chapter 2 provides the overview of the experimental setup for the research presented in this thesis. Chapter 3 provides and discusses the process planning and methodology used for the results shown in Chapter 4. Chapter 4 presents the experimental results with multiple test cases in section 4.2.1, 4.2.2 and 4.2.3. Finally, Chapter 5 provides a conclusion of the research presented herein and scope of the future work. The majority of the content is composed of previous work (Yayue Pan, Abhishek Patil, Ping Guo, Chi Zhou. "*A Novel Projection based Electro-Stereolithography (PES) Process for Production of 3D Polymer-particle Composite Objects"*, Accepted and Forthcoming in Rapid Prototyping Journal, DOI: 10.1108/RPJ-02-2016-0030.) for which I was the co-author. My advisor, Dr. Yayue Pan supervised the research and edited the manuscripts and Dr. Chi Zhou and Dr. Ping Guo aided in process design and experiment design.

TABLE OF CONTENTS

LIST OF FIGURES

LIST OF TABLES

LIST OF ABBREVIATIONS

PES	=	Projection based Electro-Stereolithography
AM	=	Additive Manufacturing
SFF	=	Solid Freeform Fabrication
3D	=	Three-Dimensional
SL	=	Stereolithography
PCL	=	Polycaprolactone
PED	=	Precision Extrusion Deposition
DDD	=	Drug Delivery Devices
DMD	=	Digital Micromirror Device
MIP-SL	=	Mask Image Projection Stereolithography
PDMS	=	Polydimethylsiloxane
LDI	=	Layered Depth Image
C_d	=	Curing Depth
D_p	=	Penetration Depth
E_c	=	Critical Exposure
T_c	=	Critical Curing Time
t	=	Curing Time
SLS	=	Selective Laser Sintering

M^2SLS	=	Multiple Material Selective Laser Sintering
STL	=	STereoLithography
2D	=	Two-Dimensional
GUI	=	Graphical User Interface
DLP	=	Digital Light Processing
CAD	=	Computer-aided Design

SUMMARY

Polymer-particle composites have been investigated for decades. They have demonstrated wide applications ranging from energy harvesting and storage, biomedical applications, electronics, and environmental sensing to aerospace applications. However, fabricating polymer particle composites with controlled distribution of particles in polymer continues to be a fundamental challenge. As to date, a few additive manufacturing technologies are able to fabricate composites, however, with a limited choice of materials or limited dispersion control. Against this background, this thesis investigates a hybrid polymer-particle composite manufacturing process called Projection based Electro-Stereolithography (PES) process, which integrates electrostatic deposition and projection based stereolithography technologies.

In PES, a photoconductive film collects charged particles in the regions illuminated by light. Then collected particles are transferred from the film to a polymer layer with defined patterns. Lastly, a digital mask is used to pattern the light irradiation of the DMD chip, selectively curing the photopolymer liquid resin and particles of that layer. By transferring particles from the photoconductive film to the photopolymer in a projection based stereolithography system, multi-material composites with local controlled dispersions could be produced. A proof-of-concept PES test bed was developed. Various test cases have been performed to verify the feasibility and effectiveness of the developed approach.

Challenges in this novel additive manufacturing process, including process design, particle patterning and transferring and polymer-particle curing are addressed in this thesis. It is found that particles can be transferred to a layer of partially cured resin completely and accurately, by using an elastomeric stamping approach. The transferring rate is related to the stamping force applied and degree of curing of the recipient layer. The developed hybrid process can fabricate high resolution polymer-particle composites with arbitrary dispersion patterns, unconstrained print heights and complicated geometries.

Although electrostatic deposition process has been investigated as a 3D printing technology for many years, it is the first attempt to integrate it with a projection based stereolithography (SL) process for fabricating multi-material polymer composite components. The novel hybrid process offers unique benefits including local dispersion control, arbitrary filling patterns, a wide range of materials, indefinite printable height and arbitrary complicated geometries.

CHAPTER 1. INTRODUCTION

[Parts of the content in this chapter is composed of previous work: Yayue Pan, Abhishek Patil, Ping Guo, Chi Zhou. "*A Novel Projection based Electro-Stereolithography (PES) Process for Production of 3D Polymer-particle Composite Objects"*, Accepted and Forthcoming in Rapid Prototyping Journal, DOI: 10.1108/RPJ-02-2016-0030.]

1.1. Background

Additive Manufacturing (AM), which is also known as 3D printing or solid freeform fabrication, is a class of technologies that builds parts layer by layer using digital 3D design data [1]. In past decades, intensive research attempts have been made to improve its manufacturing capability, in terms of speed [2, 3], surface quality [4-6], material property [7-9], process reliability [8], etc. Compared to traditional manufacturing technologies, AM offers many exclusive advantages in terms of material efficiency, simple operating style, better design flexibility, and so on [10]. Many industries have adopted AM in fabricating plastic and metal parts for various applications. However, the adoption of AM technologies as a means for fabricating end-use components is still limited by the lack of AM materials. Material choices suitable for AM are far more limited than with traditional manufacturing processes [11].

Additive Manufacturing (AM) of multi-material composites has attracted considerable research interest. In order to expand material selections, a few of composite AM technologies have been developed recently. For example, commercial machines like the Objet Connex 3D printer from Stratasys and ProJet 5500 from 3D Systems have recently entered into the market with the capability of printing multiple photopolymers in one build. As many as 14 different materials can be produced in a single printed part, by combining two base materials in specific concentrations and structures [12]. Both of them utilize the multi-jet printing process, which has unique advantage in combining materials and scalability. Yet it only accepts liquid photopolymers

and the selection of materials are constrained by their flow ability in the inkjet print head. In addition to jetting technique, some other AM techniques have also been investigated, such as multi-nozzle deposition [13], multi-vat photopolymerization [14], selective laser sintering of multi-metallic-materials [15-18]. Those research attempts made it feasible to fabricate 3D multi-polymer or multi-metal composite parts using AM principles. In contrast, few techniques have been developed for fabricating polymer-particle composites. Current additive manufacturing techniques for polymer-particle composites are usually based on solidifying a suspension of metallic/polymer particles and liquid, which is usually prepared by blending and hence has little control on local dispersion [19-21].

Polymer-particle composites have demonstrated wide applications ranging from energy harvesting and storage, biomedical applications, electronics, and environmental sensing to aerospace applications [22-25]. However, fabricating polymer particle composites with controlled distribution of particles in a host polymer material continues to be a fundamental challenge [26]. To address such a significant challenge, our research explores the feasibility of developing a hybrid additive manufacturing process by integrating electrostatic deposition with Stereolithography (SL) process.

Electrostatic deposition has been investigated and successfully developed as a 3D printing technique by researchers including Kumar group at Univ. of Florida, Cormier groups at North Carolina State University and Rochester Institute of Technology [27-35]. The capability of depositing multiple particles (polymers, metals, etc.) has been demonstrated in these pioneer works. 3D objects have been successfully printed with both metal particles like iron powders and polymer particles like nylon powders. Challenges have also been identified, including particle transfer mechanisms, distortions occurred during fusing and compaction, surface defects due to residual charges, and limited printable height.

Unlike these pioneer studies on electrostatic deposition based 3D printing, this thesis aims on fabrication of polymer-particle composite parts, instead of single-material parts. Additionally, this thesis explores a hybrid process that integrates electrostatic deposition with the stereolithography process. In the hybrid process, electrostatic deposition is used only for 2D patterning of particle deposition, while the 3D structure is achieved by the stereolithography approach. Therefore, advantages of electrostatic deposition in depositing metal/polymer/ceramic particles with programmed patterns is fully utilized, while challenges identified in others' work, such as surface defects and limited printable height are avoided in the proposed process. Chapter 2 describes the whole process, hardware and software in detail. Chapter 3 discusses particle deposition and transfer in the PES process, followed by Chapter 4 in which test cases are presented and experimental results are analyzed. Conclusions and future work are presented in Chapter 5.

1.2. Literature Review of Current Multi-Material AM Technologies

Most of the commercially available multi-material composite machines use the multi-jet printing or MJP process. In this printing process, a photo-curable plastic resin or casting wax materials are extruded or deposited layer by layer from a printed head using a piezo print head technology. 3D Systems uses this technology to build multi-material composites to address an extensive range of applications. One of the main advantages of this MJP is that it makes the post-processing process easy and hands-free operation as the support material used here is mostly separate, dissolvable, thus making the cleaning process very easygoing keeping the complicated internal cavities and delicate features intact. It also has the ability to print parts with layer thickness as low as 16 microns with higher Z-direction resolution. 3D Systems 3D printers using the MJP technology are: ProJet MJP 3600 Series, ProJet 5000 and ProJet 5500X [36].

Though the durability of plastics is improving, it is still in question and this technique finds acceptance only in some end-use applications. Stratasys also uses a similar technology called

PolyJet technology to build multi-material by jetting curable liquid photopolymer onto the build tray. Both these techniques are similar to the ink jet printing process, but instead of dropping particles of ink on the paper they extrude liquid photopolymer. PolyJet technology also produces smooth, accurate prototypes with complicate shape and intricate details with support materials which can be removed using hand or water jet [37].

Figure 1: - (a) A prototype printed by Stratasys using magenta, cyan and rubber like materials (b A multi-material 3D printed industrial part from 3D Systems ProJet 5500X machine (Pictures taken from [38] [39])

Connex 3D printers can jet up to three model materials simultaneously which can be combined to create digital materials. By doing this, one can achieve a good range of colors and hues and also varying material properties from rigid to opaque and clear to opaque. The multi-material 3D printing technology employed by Stratasys employs mainly three options of printing: Mixed tray, Mixed part, and Digital Materials. The multi-material applications for such 3d printing technologies include over molding, rubber simulation, medical devices, human organ models, display panels and sunglass lenses [37]. However, multi-material printing technologies like MJP and PolyJet printing technologies that are based on ink jet printing technology have limited use of materials as they are constrained by their ability to flow in the print heads of the printer and mostly only different colored photopolymers can be combined that too in a liquid state. Therefore, we cannot combine different metal, polymer, ceramic etc. with liquid photopolymer.

Other technique explored for multi-material printing is multi-nozzle deposition for 3D biopolymer tissue scaffold printing. This technique enables extrusion of biopolymer solutions and living cells simultaneously with scaffold construction to from complex cell-seeded tissue constructs mainly based on sodium alginate solutions and poly-ε-caprolactone (PCL). This deposition system uses four different kinds of micro-nozzles to extrude: pneumatic micro-valve, piezoelectric nozzle, solenoid valve, and precision extrusion deposition (PED) nozzle. Thus, this process is able to produce multi-polymer composites, which have wide in tissue engineering applications [13].

A multi-material mask image projection based Stereolithography process was developed by [14], in which they combined two different base materials with different structures and concentrations to produce a new material with required characteristics. This process allows production of 3D multi-material specimens with better spatial control over placement of both the material and structure. This study explores multi-vat photopolymerization for building objects with different colors and mechanical properties.

Multiple materials selective laser sintering (M^2SLS) proposed by [40, 41], manufactures multiple material freeform components separated by functionally graded interfaces. Application of such production techniques can be found in casting for producing complex sand core geometries with hollow features.

Further dual material rapid prototyping techniques have been developed by [15, 16] for development of biomedical devices (polymeric drug delivery devices). Their work produces dual material specimens by employing two process models based on Selective Laser Sintering (SLS). These process models for polymeric drug delivery device fabrication can be integrated to generate a dual or multi-material fabrication technique. The first proposed SLS based process model used a technique where a space is created during the heat sintering process by changing the density of the first material, thus creating channels where second material can be deposited.

The second process model uses an electrostatic deposition technique based on the electrophotography process for powder deposition. This technique finds application in production of drug delivery devices, as when both process models are combined it is possible fabricate dual material custom-built polymeric matrix-controlled drug delivery devices (DDD's). Although this process successfully achieves the purpose of dual material printing, it is restricted to choice of materials based on the application in production of DDD's and does not explore multiple class material printing. Moreover, the process undertakes powder deposition on a paper of thickness 50mm, thus the transfer quality highly depends on the efficiency of powder removal and transfer, printing speed and traversing speed during deposition.

Extensive research has been conducted on electrophotographic freeform fabrication techniques. Electrophotographic printing of part and binder powders was explored by Kumar *et al.*, 2003; Kumar and Dutta, 2003; Kumar *et al.*, 2004; Kumar and Dutta, 2004 [28-30], [32], wherein small components of polymer toner powder were printed using two methods: direct part printing where each layer is thermally fused with the use of a hot compaction plate and printing a part onto a part powder using a binder powder using electrophotography process. Cormier *et al.*, 2000 carried out experiments to incorporate electrophotography based layer manufacturing technique but found out to have substantial technological challenges like, efficiency of transferring the printed image from photoconductor to part/paper of greater thickness and application/removal of the support material [34]. Das, 2004 presented an investigative study of printing polymer and metal powders using a electrophotographic based rapid prototyping technique [33].

1.3. Motivation for Present Research Work

For a long time now, materials have been identified as one of the principal limitations of additive manufacturing (AM). The capability to additively manufacture multi-material parts does exist today and is paving way for unparalleled opportunities. The rapid prototyping techniques talked about in the previous section led to the idea of current research work. Currently there is a

restricted spectrum of plastics, metals and polymers available for AM platforms, with ceramics just beginning to make an advancement. In most of the cases, the research idea of integrating either of metallic, polymer or ceramic powder with liquid photopolymer has not been explored extensively and the material option still need to be augmented and amplified through the ability to combine the different material types. In addition, multi-material 3D printing has been understood to be a generic process, which involves different combination of different materials. However, with the ability to control the dispersion pattern of the metal, polymer or ceramic particles with liquid photopolymer, we would successfully be able to develop composites that haven proven wide-ranging applications from energy harvesting and storage, biomedical applications, electronics, and environmental sensing to aerospace applications. Furthermore, this thesis provides an inexpensive technique to print multi-material composites with the option of selective coloring and desired deposition patterns. Also past works on the development of electrophotographic technology were carried out mainly to check the feasibility of this technology and study its behavior for printing multiple layers of toner powder.

The proposed hybrid process utilizes the advantages of both, electrostatic deposition as well as stereolithography process, which has not been explored in the past. The starting motivation of this project was to study the feasibility of this hybrid PES process to fabricate composites and thus we started with production of specimens with toner powder and liquid photopolymer combination. To summarize, the current thesis work presents the effort to develop and print toner powder with desired deposition pattern on the cured liquid photopolymer surface. The physical properties of the powder were studied and their suitability to be used as a structural material would ultimately lead way to the use of ceramic, polymer and metal particles.

1.4. Conventional Projection based Stereolithography System

Stereolithography (SL) is a widely used rapid prototyping techniques to manufacture models layer by layer using photo-polymerization process. A 3D CAD design is generated in the

form of a STL file, which is further sliced layer-by-layer with the use of 3D printing software. These sliced images are then projected through a projection unit (in the form of an ultraviolet laser beam), which uses a bulb as the light source and DMD chip which patterns the light. The laser beam traces the sliced image pattern on the surface of a liquid photopolymer/resin. Exposure of the surface of this liquid photopolymer to the laser beam solidifies the pattern traced on the resin and joins it to the subsequent layer. There are two SL projection systems: bottom-up projection and top-down projection. Top-down SL projection system is employed here rather than bottom-up projection because of its reliability and simplicity. In SL apparatus, we are able to achieve high surface quality finish, better dimensional accuracy, and a range of material options by using a laser and a liquid photopolymer. Figure 2 illustrates the schematic of a top-down Mask Image Projection base Stereolithography (MIP-SL) system.

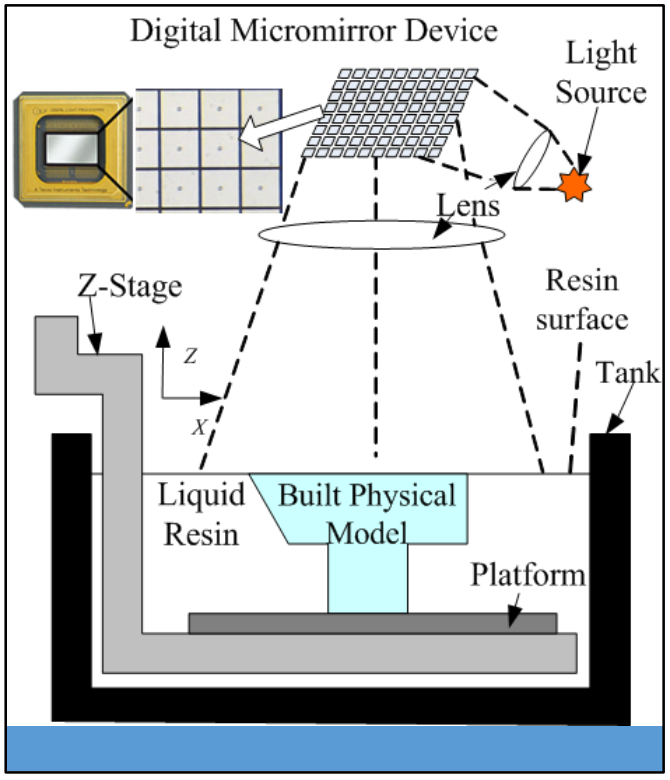

Figure 2: Illustration of a top-down Mask Image Projection based SL system (Picture taken from [42])

1.5. Research Scope

The scope of this research work is shown below in a schematic illustration. This research work focused on polymer-particle composite 3D printing, explored the feasibility of printing multi-class particle composition using materials like metal, ceramic and polymer together. This study investigated various mechanism of integrating particle deposition in polymer (resin) cured and uncured models. The study involved in-depth analysis of the curing mechanics of the polymer-particle slurry and behavior of different parameters like weight ratio, particle size, curing time, density etc. to explore this behavior. Different hardware prototype designs were considered to efficiently integrate the electrostatic deposition and SL processes. Various motion controllers like Dynomotion's KFlop and Arduino were considered according to their ease of use and efficiency, for controlling the linear actuators. In the end, several test cases were printed with controlled deposition of toner particles, to investigate the mechanical properties of the 3D printed composite, the feasibility and capability of PES process. Figure 3 summarizes the scope and flow of this thesis study.

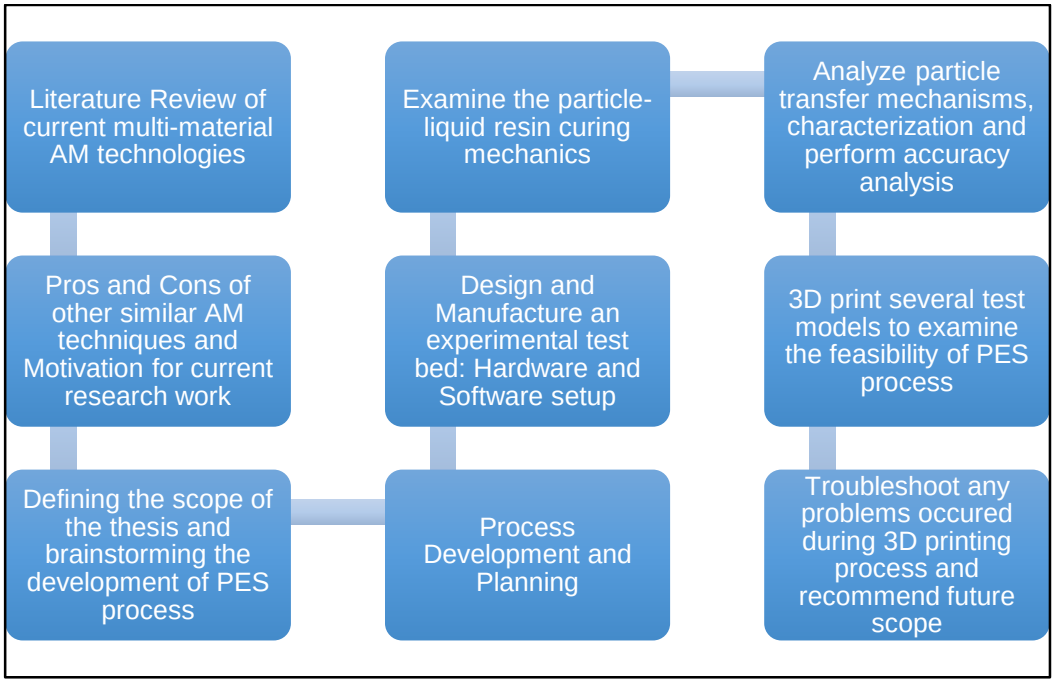

Figure 3: Research scope of this thesis study

1.6. Summary

The INTRODUCTION chapter reviewed various multi-material additive manufacturing technologies currently in the market and some promising applications of multi-material 3D printing. Advantages and disadvantages of current multi-material composite manufacturing techniques are examined and reviewed, which led to the idea of a novel process, Projection-based Electro-Stereolithography (PES). Lastly, the research scope and flow of this thesis study are established and demonstrated.

CHAPTER 2. DEVELOPMENT OF PES PROCESS

[The majority of the content in this chapter is composed of previous work: “Yayue Pan, Abhishek Patil, Ping Guo, Chi Zhou. *A Novel Projection based Electro-Stereolithography (PES) Process for Production of 3D Polymer-Particle Composite Objects*”, Accepted and Forthcoming in Rapid Prototyping Journal, DOI: 10.1108/RPJ-02-2016-0030.]

2.1. Overview of PES Process

Projection Stereolithography technology offers high material resolution, dimensional accuracy and good surface quality. By using a DLP projector and liquid photo curable resin, we can define and control the pattern of the images that will be projected on a surface area and in turn, control the shape of the cured layer. On another hand, electrostatic deposition digital printing, also known as electrophotographic printing, has achieved a high level of productivity and maturity in mainstream 2D printing, and thus the feasibility of 3D printing has been demonstrated [27]. However, the majority of the pioneer work has been done by incorporating electrophotography into a powder-bed fusion system, which suffers from limited build height problems and fusing distortions [27-30].

In this study, the proposed Projection based Electro-Stereolithography (PES) process consists three steps- (a) electrostatic deposition of particles with a certain pattern, (b) transferring of particles to photopolymer, and (c) photo-curing of polymer-particle composites. Specifically, a photo curable resin and metal/polymer particles are used as the feedstock. Digital masks are used in both the particle deposition part and photo-curing part. The proposed PES approach opens up new ways of controlling material distributions and processing by incorporating the electrostatic deposition mechanism into a stereolithography based AM process. Specifically, the configuration of PES system is shown in Figure 4 and the process follows seven main steps:

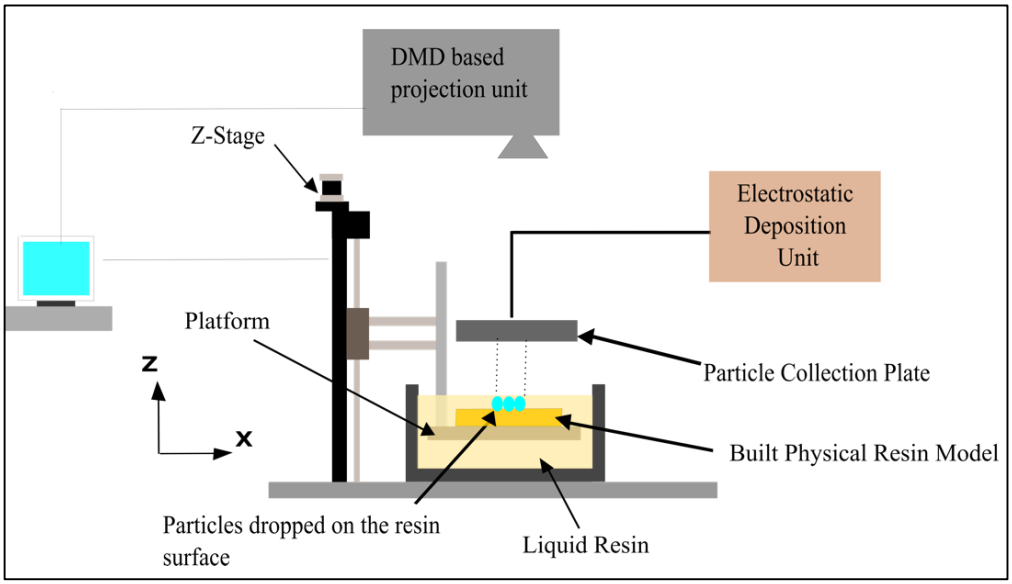

Figure 4: Illustration of Projection based Electro-Stereolithography (PES) process

(1) Initialization: the 3D digital model is loaded in the process control software, and sliced into two sets of 2D images: one for liquid resin photo-curing (image set L) and the other for particle patterning (image set P). The platform and the particle collecting plate are homed. The projection and the electrostatic deposition units are initialized.

(2) Curing: the resin curing image of that layer in the image set L (photo-curing set) is projected to the photopolymer, to selectively cure the resin of that layer.

(3) Charging: in the electrostatic deposition unit, the photoconductor surface is negatively sensitized with electrostatic charging by means of a corona charging device or charging roller for the toner cartridge.

(4) Exposing: in the electrostatic deposition unit, the photoconductor surface is scanned by the laser beam, which discharges the photoconductor and forms a latent image according to the particle deposition image of that layer (from image set P).

(5) Particle Collection: in the electrostatic deposition unit, the developed image is then transferred to the particle collection plate. The charging roller positively charges the plate and the electrostatic force attracts the toner powder to jump on to the plate.

(6) Particle Transfer: the charged particle collection plate is then moved to the surface of liquid resin by using two linear stages. Particles are then transferred to the photopolymer by stamping transfer method (which is discussed in detail in Section 3.2).

(7) 2^{nd}-Curing: the current layer of resin curing image from image set L is projected again to fuse the newly transferred particles.

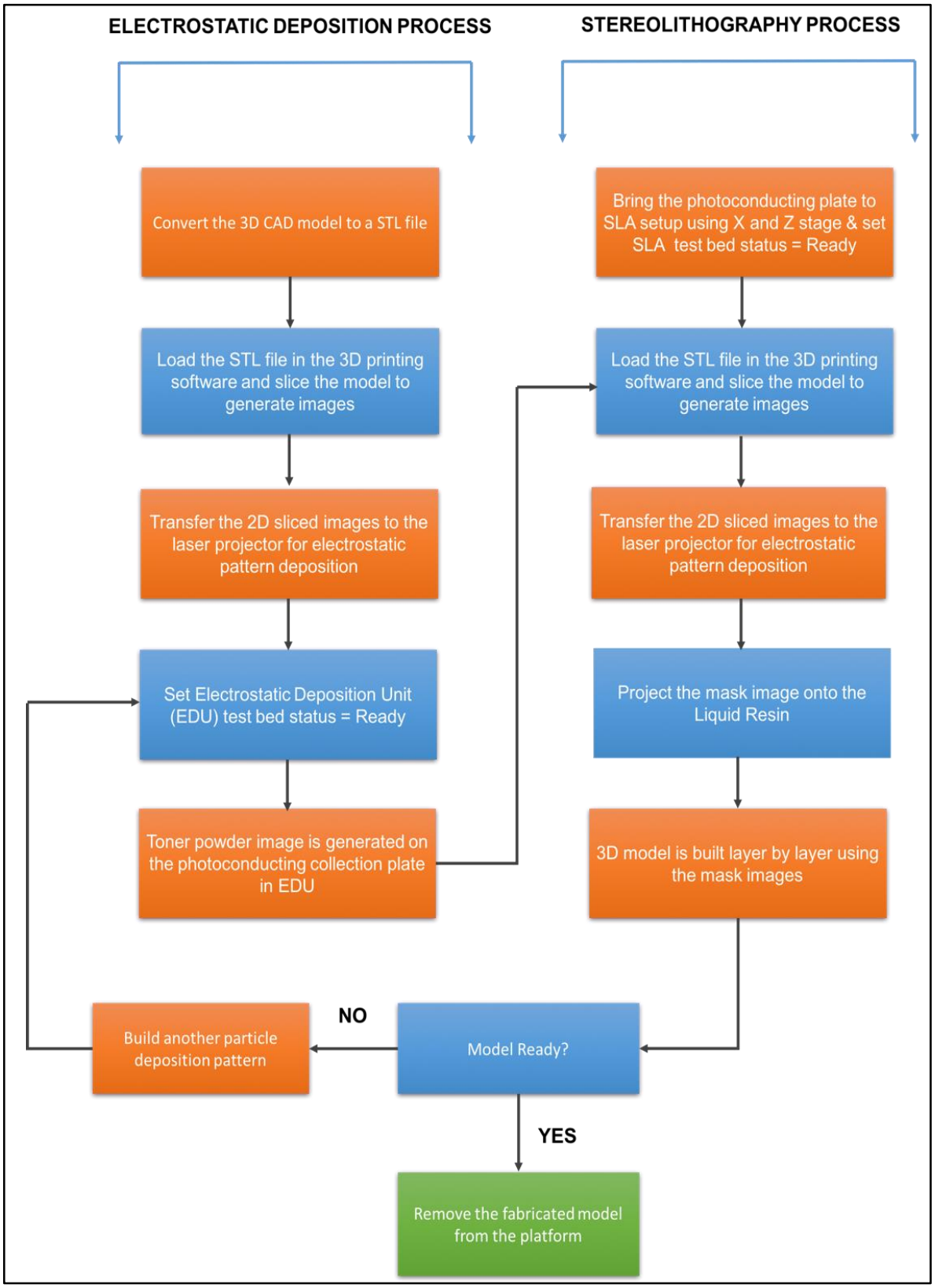

Figure 5: Flowchart of working of the PES system

2.2. Software Setup

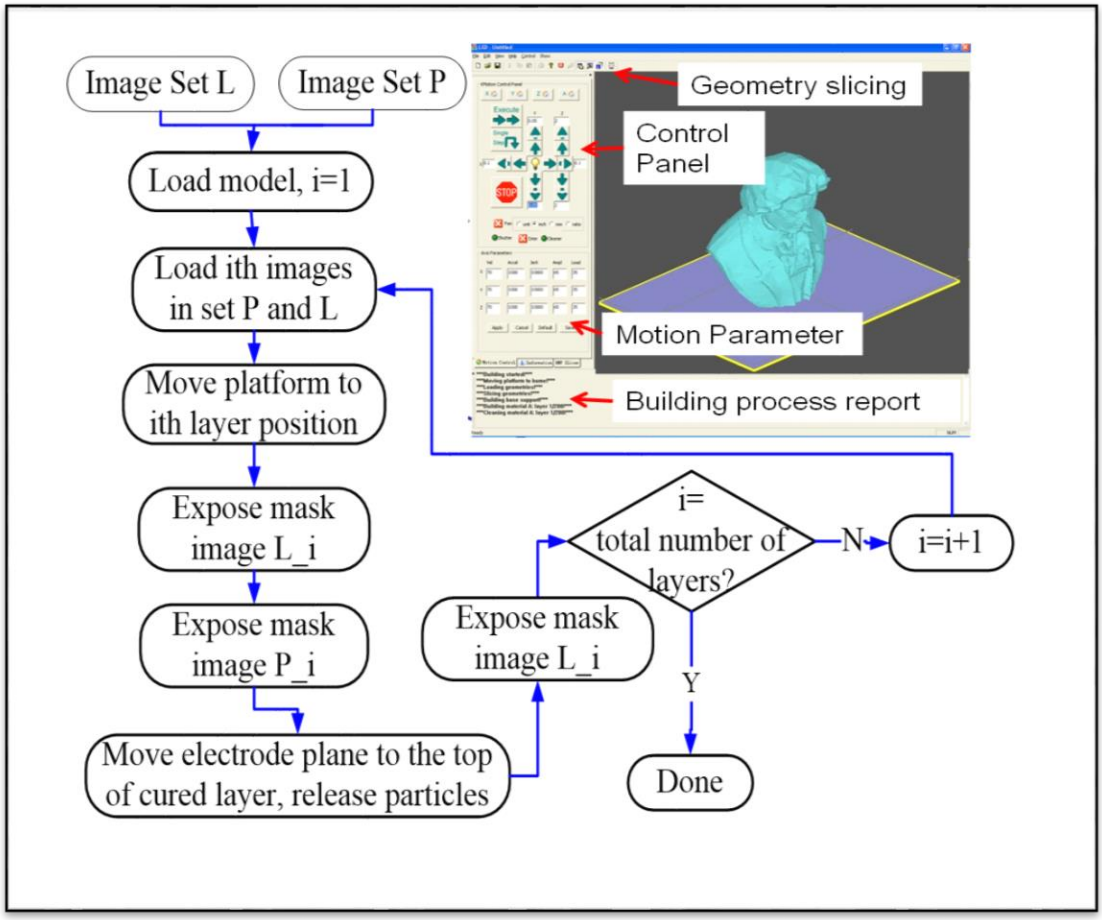

Figure 6: Flow chart and graphical user interface (GUI) of the developed software system

A mask image planning test bed has been developed using the C++ language. It integrates the geometry slicing, digital mask generation, image loading, projection and motion controlling. Digital masks are constructed according to the material distribution of the sliced layer. Mask image projection is synchronized with the movement of the z-stage driving the build platform. The flow chart of the PES process and the graphical user interface (GUI) of the test bed is shown in Figure 6. There are two different sets of STL file “Image Set L’ and ‘Image Set P’ and we have the choice of exposing either of the image sets first, based on the fact that the particles are transferred on to the cured resin surface or uncured resin surface

2.3. Hardware Setup

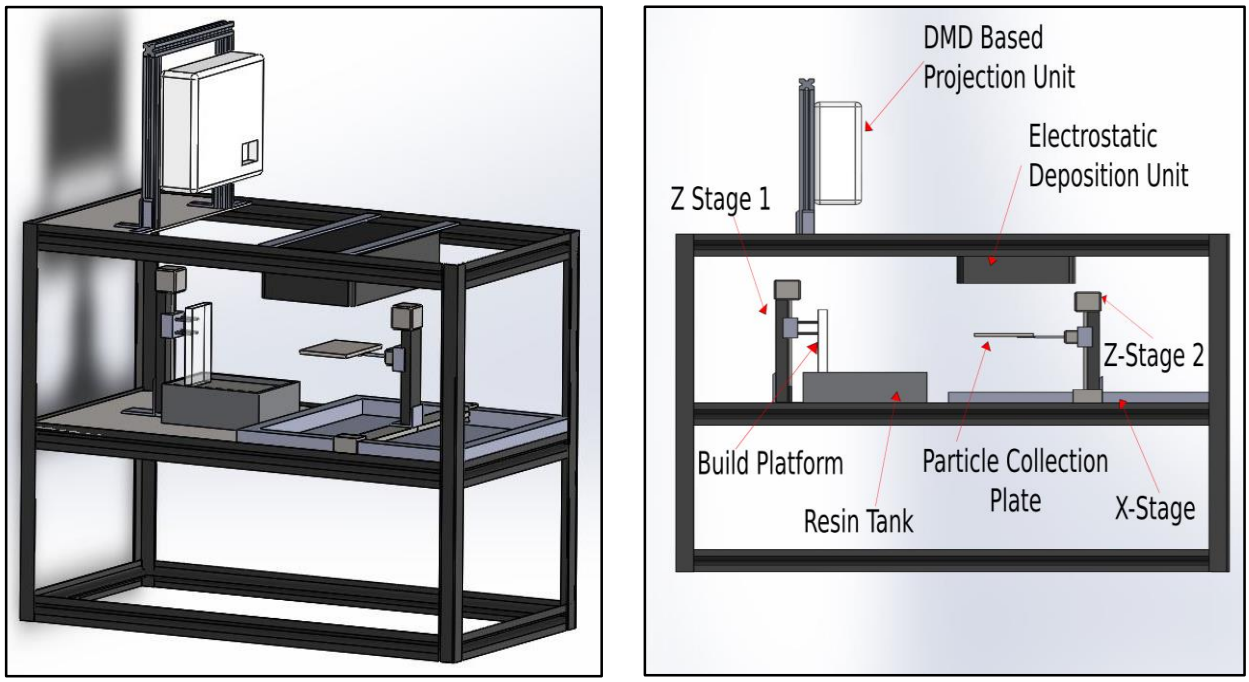

***Figure 7**: (a) 3D View of the hardware system design, (b) Side view of the hardware setup depicting the EDU and SL units*

A prototype machine has been developed, as shown in Figure 7. To reduce the prototype cost and simplify the system design, an off-the-shelf projector (Acer H6510BD) was modified and used as a DLP projection unit. Various projection settings including focus, key stone rectification, brightness and contrast have been adjusted to achieve a sharp projection image on the designed projection plane. The DMD resolution in our system is 1024×768 and the envelope size is set at 5.35 by 4.06 inches. Three precise linear motion stages from Oriental Motor U.S.A. Co. (Elk Grove Village, IL) are used to drive the platform and the particle collecting plate. In the electrostatic deposition unit, a photoconductive film is used to collect charged particles on a plate in regions illuminated by light. The Z-stage elevator located under the DMD based projection unit drives the build platform up and down. The other two linear stages, Z-stage and the X-stage are used to

collect particles from the electrostatic deposition unit and transfer them to the built model on the build platform. A high performance 4-axis motion control board with 28 Bi-directional I/O pins from Dynomotion Inc. (Calabasas, CA) is used to drive linear stages. The electrostatic deposition unit is built from parts of an HP LaserJet (P1102w) printer. Figure 8 below shows the actual prototype hardware setup established for the purpose of carrying out experiments.

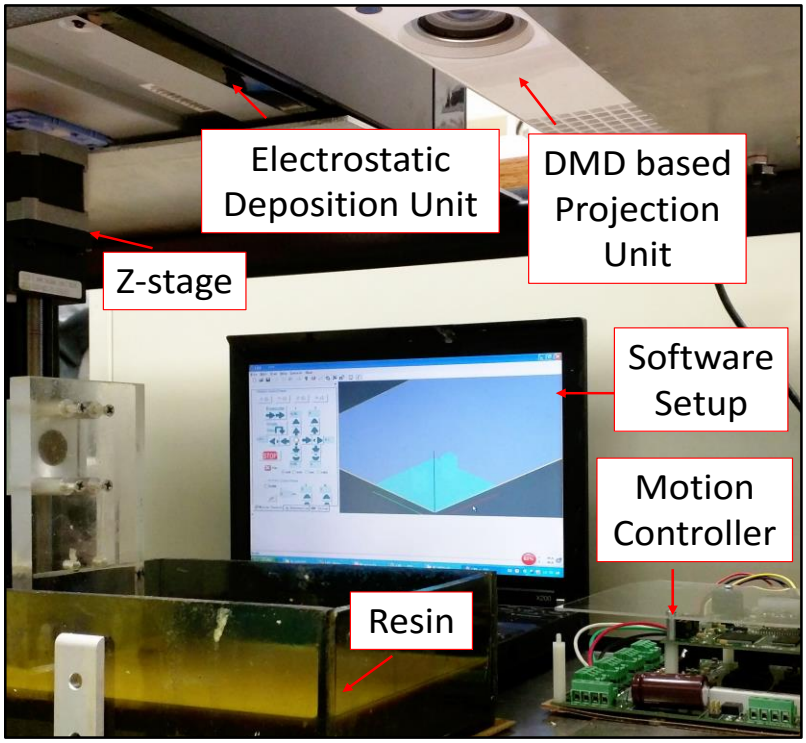

Figure 8: The developed prototype system for the PES process

2.4. Material Choice

A commercially available resin, Perfactory™ LS600M (yellow) from EnvisionTEC Inc. (Ferndale, MI), was used in testing the developed PES system. EnvisionTEC's LS600 provides high feature detail parts for use in producing accurate parts. With high surface quality and stability, we could produce parts similar to thermoplastics having a high impact resistance using this material. The material has opaque yellow-beige color with a viscosity of 140 cP at 30° and a density of 1.10 g/cm^3. In addition, the Tensile Modulus and Tensile Strength at break for this

material is 1,800 MPa and 60 MPa respectively [43]. For the LS600M resin and 152.3 μm layer thickness, it takes 15 seconds curing time to achieve 100% degree of conversion in our testbed. The particles used in the test case study for polymer-particle study are toner particles of the HP LaserJet P1102w printer (8-10 micrometers in size, 600 dots per inch resolution)

2.5. Summary

In this chapter, PES process is introduced and its working is explained in detail. The importance of projection based SL process is discussed and the integration of SL with electrostatic deposition process is explained in detailed in steps. A flowchart is presented showing the working of the PES process and the working procedure is described. Then the software setup used for controlling the linear actuator and 3D printing software, which controls the slicing parameters, is illuminated. A CAD model of the proof-of-concept hardware prototype system and the actual system is exhibited and the various components used in the hardware setup are introduced. The liquid photopolymer and toner particles used for this research work are introduced in the next section.

CHAPTER 3. PROCESS PLANNING

[Parts of the content in this chapter is composed of previous work: Yayue Pan, Abhishek Patil, Ping Guo, Chi Zhou. "*A Novel Projection based Electro-Stereolithography (PES) Process for Production of 3D Polymer-particle Composite Objects"*, Accepted and Forthcoming in Rapid Prototyping Journal, DOI: 10.1108/RPJ-02-2016-0030.]

The novel rapid prototyping process we are working on integrates electrophotography printing and projection based stereolithography process, hence requiring careful consideration of different number of parameters, which could affect the process. In electrostatic deposition, we deposit a layer of coating onto the substrate that is then transferred via a stamping transfer mechanism onto the cured photopolymer layer with desired dispersion patterns.

3.1. Particle Deposition

3.1.1. Overview of Electrostatic Deposition Technology

In electrostatic deposition process, charged powder (in our case toner particles) are arranged on a substrate according to the desired pattern which is projected by the DMD based projection unit. A special nonconductor material referred to as photoconductor is employed to create image patterns of charged or discharged areas by exploiting its special property, such that when a light of a certain wavelength is projected on it, it turns conductive [44].

The DMD based projection unit projects the input image via a Digital Micro Mirror Device (DMD), which consists of a chip that has an arrangement of several hundred thousand micro mirrors on it in the form of a rectangular array. Now these micro mirrors control the number of pixels that can be displayed in the image. These mirrors can be turned off or on by changing its orientation by individually rotating the mirrors by $\pm 10 - 12°$ [44]. In the on state, light from the projector knob is reflected into the lens making the pixel seem splendid on the screen. In the off

state, the light is coordinated somewhere else (typically onto a heatsink), making the pixel seem dark [44].

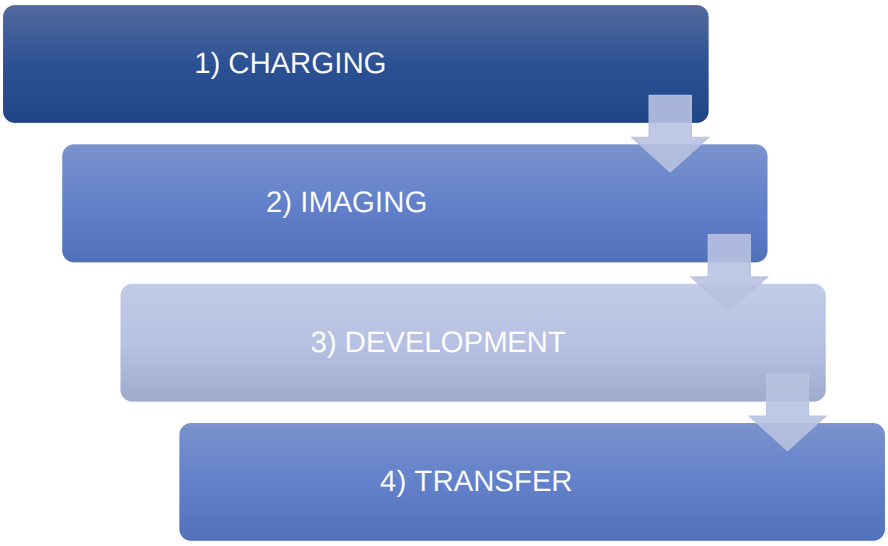

Figure 9: Flow chart of the electrostatic deposition process

The electrostatic deposition process mainly involves four major stages:

1) Charging: Here, the photoconductor drum surface is negatively sensitized by using a charging device like a corona charging device or by direct contact charging methods. For this research purpose, the photoconducting drum surface was charged using a corona charging device.

2) Exposing: In this process, light in the form of a UV laser beam of a certain wavelength is shined on the previously charged photoconducting drum surface, which discharges the photoconductor areas according to the input image and thus yields a charged image with discharged region or a discharged image with charged region

3) Development: In this phase, slack charged powder particles from the developer move towards the photoconductor drum surface because of the electrostatic force generated between

the photoconductor drum and powder. These powders get deposited image-wise on the photoconductor drum surface due to attraction or repulsion by the charged areas on the photoconductor surface.

4) Transfer: In this stage, the powder particles deposited image-wise on the photoconductor surface are transferred on to a photoelectrode substrate (collection plate) to form a permanent image [44].

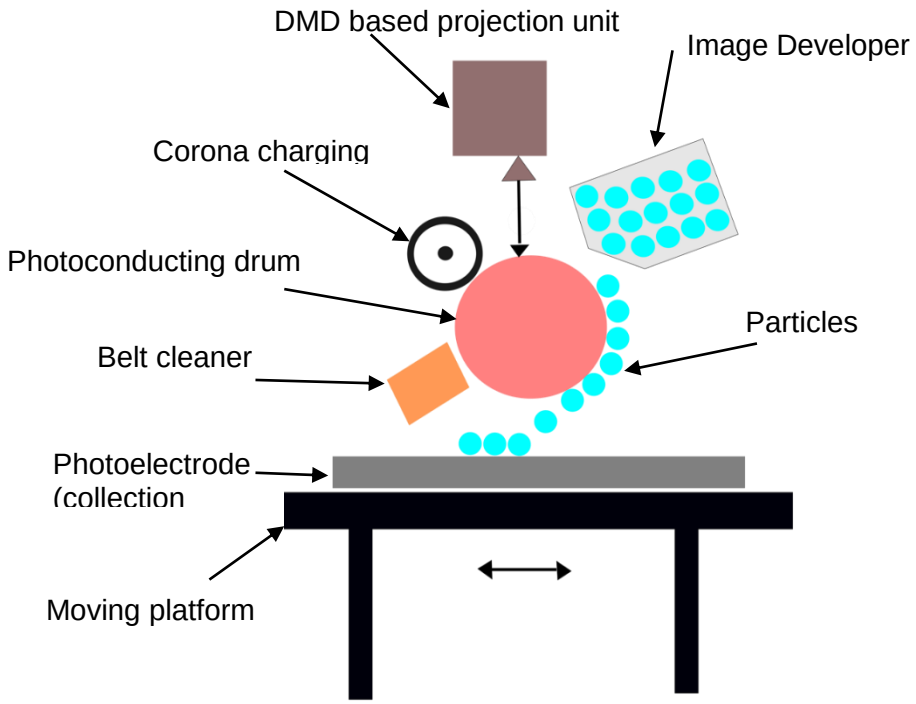

Figure 10: A schematic representation of the electrostatic deposition process

A schematic representation of the electrostatic deposition process is shown in Figure 10, which demonstrates the working of the whole process around a photoconducting drum. Most current printers use photoconducting drums for printing because it facilitates in keeping the design as compact as possible. Furthermore, the compact design makes it simpler for the printer to be used as a desktop printer. As will be seen from the electrostatic deposition print cycle, the photoconductor drum is central to this method.

After collecting the toner particles with desired deposition pattern on the photoelectrode (the collection plate), it is moved to the test-bed setup where the particles are then transferred to cured resin surface of the built part using a stamping method. This particle transfer method is talked about in detail in the next section.

3.1.2. Particle Collection Mechanism

Electrostatic digital printing, also known as electrophotography printing, is a well-established and commonly used process in 2D laser printers, where the toner is selectively deposited onto a piece of paper to produce the desired printed copy.

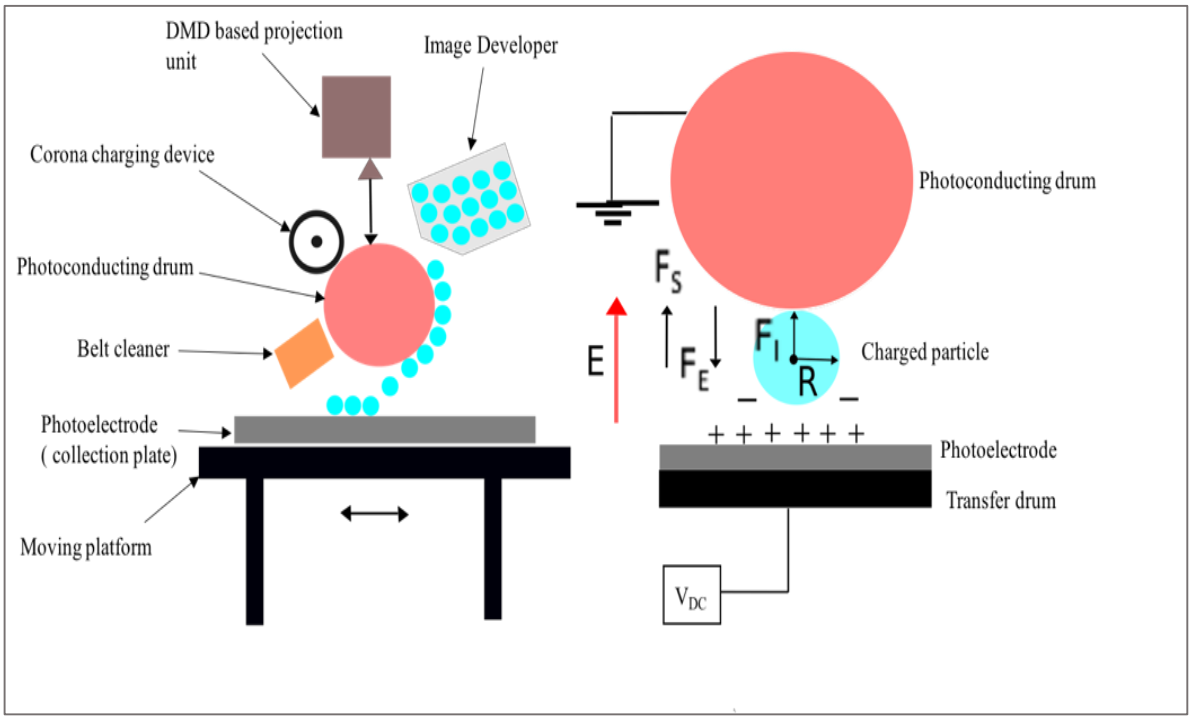

Figure 11: (a) Schematic illustration of the electrostatic deposition printing, (b) Force model for the toner-photoelectrode arrangement.

Figure 11 shows an illustration of a typical electrostatic deposition process. The photoconductive surface of the drum is charged by corona discharge. This charged photoconductive surface is then exposed to a digital mask so that the charge on the surface is

dissipated to the ground. Due to the electrostatic forces, the charged particles dropped from the image developer adhere to the surface when it is brought in vicinity of the latent image. This pattern is then transferred on to the photo-electrode with the help of an electric field. Thus, the charged particles are collected on the photo-electrode surface. Lastly, the photoconductive surface is cleaned for next particle pattern deposition.

The relationship between electric field intensity and the potential applied to the build platform is computed using Gauss Law's [31, 32]. According to the special conditions in PES process, a simplified model of electric field could be derived as:

$$E\left(\frac{p}{\sigma_S}\right) = \frac{V_{DC} + \frac{\rho_1 {d_1}^2}{2K_1\epsilon_0} - \frac{\rho_2 {d_2}^2}{2K_2\epsilon_0} + \frac{p}{\epsilon_0}(\sigma_s + \rho_1 d_1)}{K_1\left(\frac{d_1}{K_1} + \frac{d_2}{K_2} + p\right)} \quad (1)$$

In the above equation, V_{DC} is the voltage applied across the build platform; p is the height of the printed part (or previously printed layers); d_1 is the thickness of the printed powder layer; d_2 is the thickness of the photoconductive layer; K_1, K_2 are the relative permittivity of the printed powder layer and the photoconductive drum layer respectively; ρ_1, ρ_2 denote the charge per unit volume in the fresh printed layer and photoconductive drum layer respectively; σ_s is the charge per unit area deposited on the print surface and ϵ_0 is the permittivity of the air.

Now the electrostatic detachment force F_E exerted on a spherical particle having a radius R and charge q from the photoconductor by an applied field of magnitude E is given by [45, 46]:

$$F_E = \beta qE - 4\lambda\pi\epsilon_0 R^2 E^2 \quad (2)$$

In an actual scenario, however, a particle is partially surrounded by air and partially in contact with the photoconductive surface. For these conditions, it is not possible to draw a Gaussian surface around the particle, so the part of the toner particle, which is closest to the photoconductor surface, will have the greatest effect on the electrostatic attraction [45]. Hence, Equation (2) would reduce to:

$$F_E = qE \tag{3}$$

In addition, the toner particles are held to the photoconductor surfaces by two forces. The first is an electrostatic force F_1 caused by the toner particle inducing image charge within the photoconductor and is given by:

$$F_I = -\beta \frac{q^2}{4\pi\epsilon_0(2R)^2} \tag{4}$$

The second force is F_s, arising from the surface forces such as those due to van der Waal's attraction. This force is given by the Johnson-Kendall-Roberts (JKR) equation [45, 47]:

$$F_s = -\frac{3}{2}\omega_A \tag{5}$$

where ω_A is the thermodynamic work of adhesion which is related to the surface free energies of the toner particle Υ_T and photoconductor Υ_S, as well as the interfacial energy by Υ_{TS} :

$$\omega_A = \Upsilon_T + \Upsilon_S + \Upsilon_{TS} \tag{6}$$

The approximate value of ω_A for a toner particle on an organic substrate is $\omega_A \sim 0.05\ \mathrm{J/m^2}$ [48]. The force acting on the toner particle due to gravity F_W can be represented as:

$$F_W = mg = pVg \tag{7}$$

Therefore, the net force F_T acting on the particle to separate it from the photoconductive surface should be greater than zero for successful deposition of the particles on the collection plate. From equations (3), (4), (5) and (6), it could be written as:

$$\mathrm{F_T} = \mathrm{qE} + \rho\mathrm{VG} - [\mathrm{F_I} + \mathrm{F_S} + \mathrm{F_A}] > 0 \tag{8}$$

Here F_A is including all the adhesion and cohesion forces, other than van der Waals, double layer, chemical, hydrophobic forces [49].

3.2. Particle Transfer

The stamping transfer mechanism as illustrated in Figure 12 is used to transfer the particles with desired deposition patterns to the cured resin surface. In Figure 12, the present cured layer, which is supposed to be occupied with particles, is denoted by yellow color. Now the particle collection film inked with particles is stamped on the layer surface film with a particular stamping force F_s for ~2 seconds, and then with a velocity v_p, the collection film is flayed off from the layer surface. There are a number of forces to be considered when the particle collection film is flayed off the layer surface, like an upward force F_E, downward force F_a and F_g exerted on a particle. Here,

F_E = adhesion force from the collection film that prevents particles leaving from the film, mainly due to the electrostatic attraction,

F_a = adhesion force developed due to the cured layer that separates particles from the film, which is a combined result of surface tension, viscous force, mechanical interlocking, etc., depending on the stamping force and layer surface conditions, and

F_g = the downward force due to gravity

Thus to successfully transfer the desired deposition pattern from the particle collection film to the resin layer surface the net downward force should be greater than the net upward force

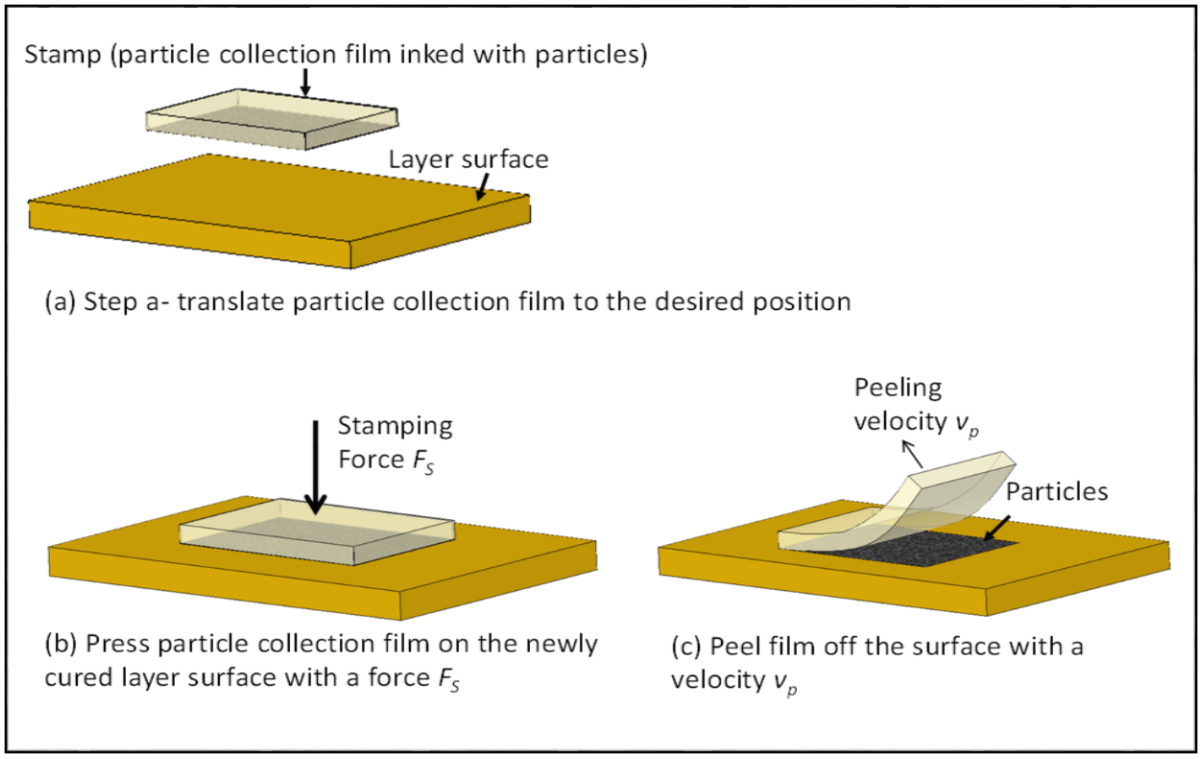

Figure 12: Particle transfer process using stamping approach

Under different conditions during the transferring process, the forces applied on a particle caused by particle-liquid interaction or particle-liquid-solid interaction are investigated which are shown in Figure 12. There is a formation of a thin film of liquid resin on the newly cured layer

surface because of oxygen inhibition. Moreover, for more efficient transferring, the amount of liquid resin on the layer surface and the degree of conversion of the layer can be adjusted in addition to controlling the curing time of the layer. Besides, a particle-liquid-solid interaction can be formed to assist the transferring, by applying appropriate stamping force and proper curing time. Now we will consider both the conditions, i.e. particle-liquid interaction and particle-liquid-solid interaction and further analyze the forces in both the conditions.

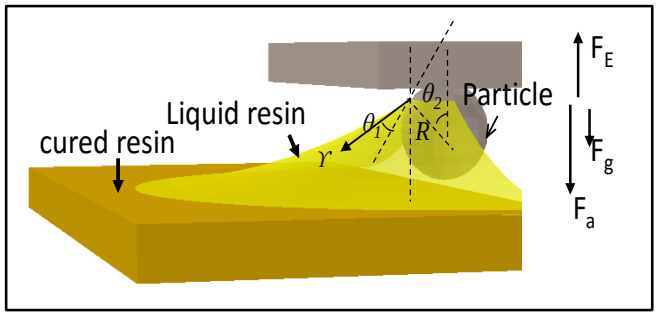

(a)

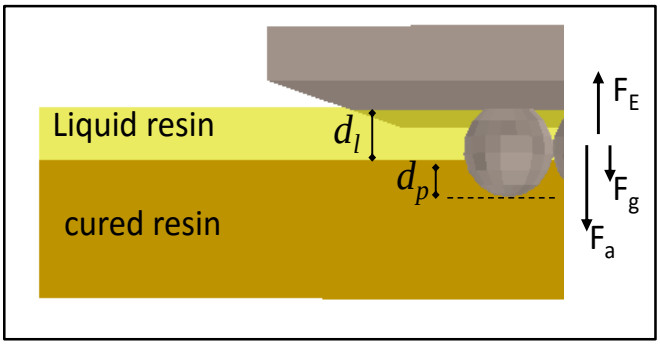

(b)

Figure 13: An illustration of the particle transfer process through elastomeric stamping: ***(a)*** **Separation process with particle-liquid interaction** ***(b)*** **Separation process with particle-liquid-solid interaction**

a) Particle –Liquid Interaction

When the transfer process involves particle-liquid interaction only, as shown in Figure 13 (a), the adhesion force F_a is mainly caused by the liquid bridge. Dynamics and rupture conditions

of liquid bridges are widely studied [50-56]. The vertical component of liquid bridge force is typically modeled by analyzing the total free energy of liquid bridge [51]:

$$F_a = \sigma \cdot l_t \cdot \sin(\theta_2 - \theta_1) + \Delta P \cdot A \tag{9}$$

where σ is the surface tension, ΔP is the difference between vapor pressure and liquid pressure, θ_1 is the contact angle, θ_2 is the deviation angle and l_t is the perimeter of the interfacial area A. Geometric relationship of these parameters is shown in Figure 13 (a). Before the liquid bridge breaks, it could be considered that the outside half of the particle forms the liquid/air/solid interfaces and the inside half of the particle is immersed within the liquid. The interfacial parameters could be approximated as:

$$l_t = \pi R \sin\theta_2 \tag{10}$$

$$A = \pi(R \sin\theta_2)^2 \tag{11}$$

$$\Delta P = \frac{2\sigma}{r_m} \tag{12}$$

where *R* is the radius of the particle, and r_m is the mean radii of the liquid interfacial profile. Substituting equation (10) (11) and (12) into (9) leads to:

$$F_a = \sigma\pi R \sin\theta_2 \left(\sin(\theta_2 - \theta_1) + \frac{2R \sin\theta_2}{r_m}\right) \tag{13}$$

It can be seen from Equation (13) that, the transferring result depends on surface tension and contact angles greatly. With given liquid resin and particles, there is little room to adjust the adhesion force to improve transferring rate. Therefore, it is desired to press particles on the surface of partially cured resin layer and utilize the particle-solid interaction for transferring.

b) Particle-Solid Interaction

As shown in Figure 13 (b), when the applied stamping force is sufficient, a particle-solid interaction will be formed. In such conditions, the adhesion force is much more complicated. Its modeling depends on many variables, such as the particle size, cured resin surface condition, liquid resin residue thickness, and chemical properties of the particle and cured resin, etc. With given resin and particle materials, variables that influence the transferring results include stamping force F_s, stamping duration t, peeling velocity v_p, and degree of conversion of the cured resin which is determined by curing time t_c. Thus by assessing these parameters one can estimate the behavior

3.3. Transferring Process Characterization

3.3.1. Transfer Process Using Collection Film

The curing time and the stamping force are supposed to have a substantial influence on the transfer rate of the particle from the collection film to the resin layer surface considering how complex the model is. In this study, toner particles and an acrylic resin LS600M from EnvisonTEC Inc. were investigated. The stamping duration was fixed at 2 seconds, peeling velocity was fixed at ~5 mm/s, and a layer thickness of 152.3 μm was used.

In the calibration experiments, particles were deposited on the collection film with a solid circle pattern and then transferred to a cured resin surface using the stamping approach. After stamping, transferred rate was calculated by approximately measuring the area that was colored by the toner on the partially or fully cured resin surface. For the LS600M resin and 152.3 μm layer thickness, it takes 15 seconds curing time to achieve 100% degree of conversion in our testbed.

To calibrate the influence of cured layer condition, particles transferring tests were performed with a stamping force of 120 N on different cured resin surfaces that were fabricated by using curing time varied from 5 s to 15 s. In Figure 14 (a), we can see the test cases with

different transfer rates of the toner particles. Measured transfer rates are plotted in Figure 14 (b). It is clear that the transfer rate increases with the curing time, however, when the curing time reaches a certain point, the transfer rate decreases as the curing time increases. For the materials in our tests, a curing time of 9 seconds gives the best transferring performance.

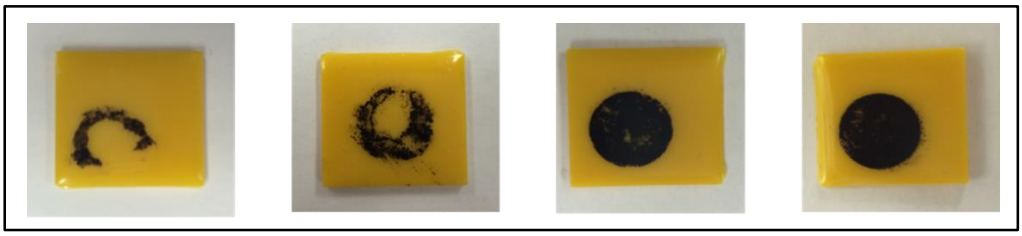

(a)

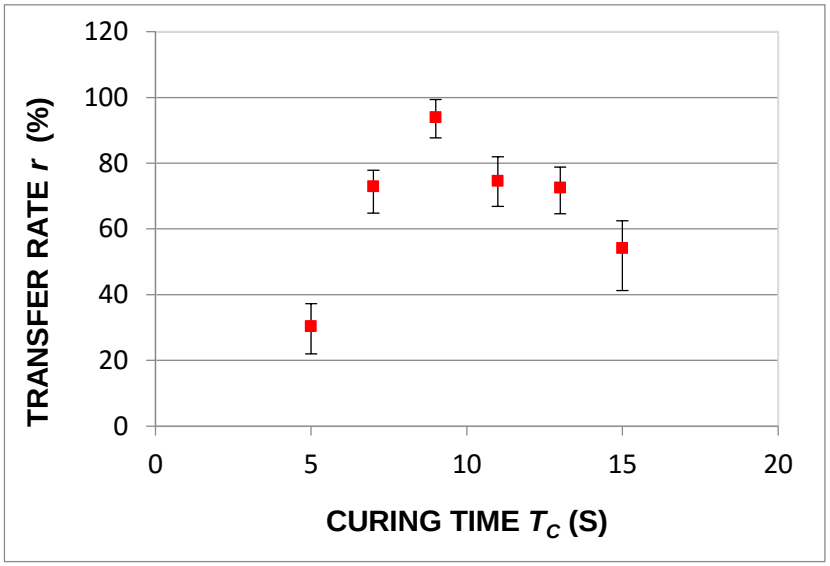

(b)

***Figure 14**: (a) Test samples with varied transfer rates (b) Transfer rate vs. curing time plot for transfer of toner particles*

Transferring tests were also conducted by applying a stamping force varied from 27 N to 158 N on resin surfaces that were cured by a curing time of 9 seconds to see how it affects the transfer rate. Figure 15 (a) shows the test cases with different values of applied force starting from 102.82N to 148.32N, and we can see that as we increase the force applied the transfer rate increases. The transfer rates with varied applied transfer force are plotted in Figure 15 (b). It is

found that the transfer rate increases almost linearly with stamping forces in the early range, i.e. from 27 N to 110N. After the transfer rate approaches its maximum value, the increasing rate gets smaller.

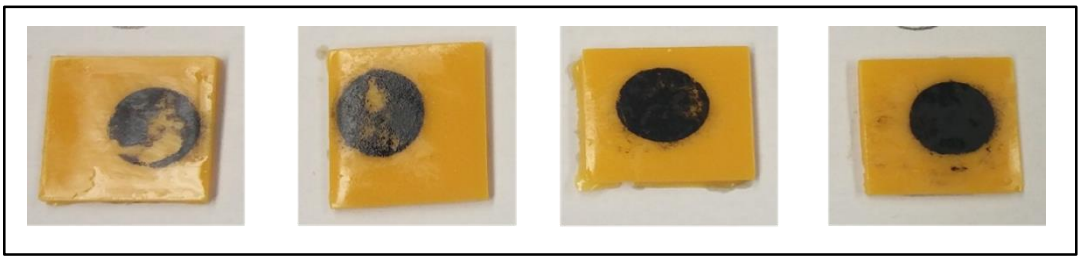

(a)

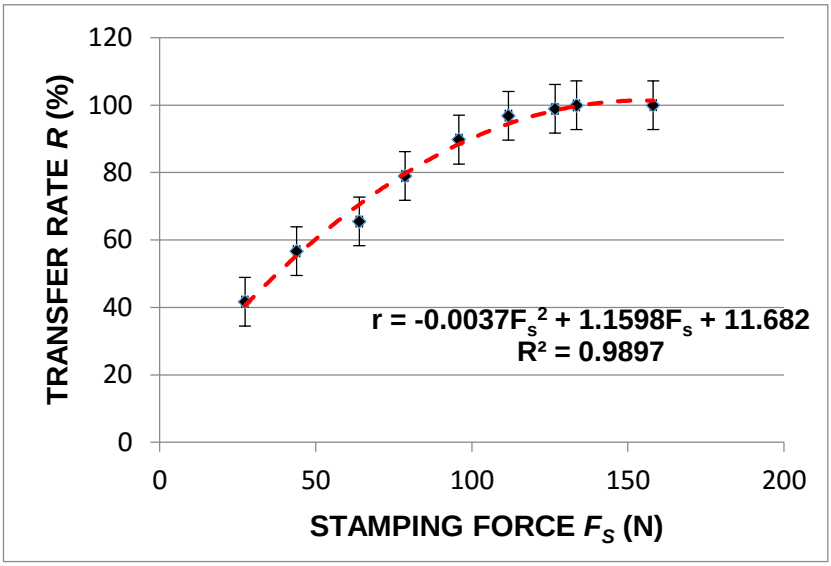

(b)

Figure 15: (a) Test samples with varied applied force for transfer characterization study (b) Transfer rate vs. stamping force plot

3.3.2. Transfer Process Using PDMS (Polydimethylsiloxane) Film

In the previous sections we studied the transfer rate characterization for transfer of the toner particles from the paper based collection film to resin layer. In this section we will be transfer the pattern from a PDMS film to the resin layer. We simply replace the previous collection film with a new collection film with a thin layer of PDMS deposited on it, with thickness close to ~ mm.

The properties of the PDMS allow us to have a com parable deposition pattern accumulated on the PDMS film instead of a paper based collection film as in the previous section. So here we discuss the transfer process characterization analysis for the transfer from the PDMS film to resin layer using the toner particles and an acrylic resin LS600M from EnvisonTEC Inc. (same as used in the previous sections). The stamping duration was fixed at 3 seconds, peeling velocity was fixed at ~5 mm/s, and a layer thickness of 152.3 μm was used.

In the calibration experiments, particles were deposited on the collection film with a solid circle pattern and then transferred to a cured resin surface using the previously employed stamping approach. After stamping, transferred rate was calculated by approximately measuring the area that was colored by the toner on the partially or fully cured resin surface. For the LS600M resin and 152.3 μm layer thickness, it takes 15 seconds curing time to achieve 100% degree of conversion in our testbed.

To calibrate the influence of cured layer condition, particles transferring tests were performed with a stamping force of 120 N on different cured resin surfaces that were fabricated by using curing time varied from 5 s to 15 s. Figure 16 (a) shows test cases with 3 different values of curing time. Measured transfer rates are plotted in Figure 16 (a). It is clear that the transfer rate increases with the curing time, however, when the curing time reaches a certain point, the transfer rate decreases as the curing time increases. For the materials in our tests in this case, a curing time of 7 seconds gives the best transferring performance.

(a)

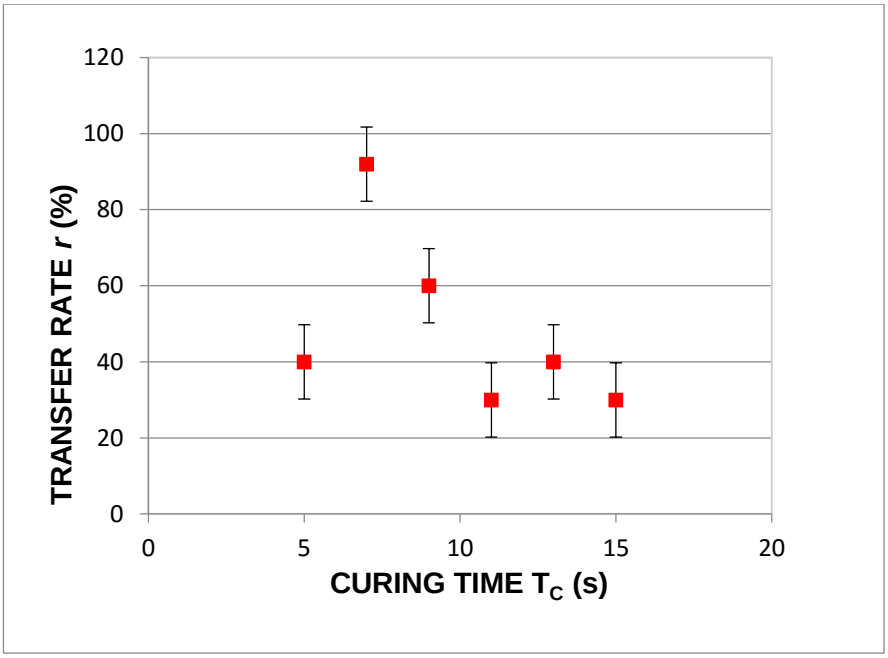

(b)

Figure 16: (a) Test samples with varied transfer rate with different curing times (b) Transfer rate vs. curing time plot for transfer of toner particles

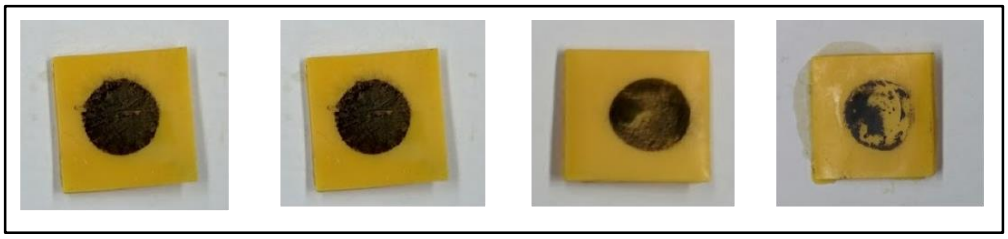

(a)

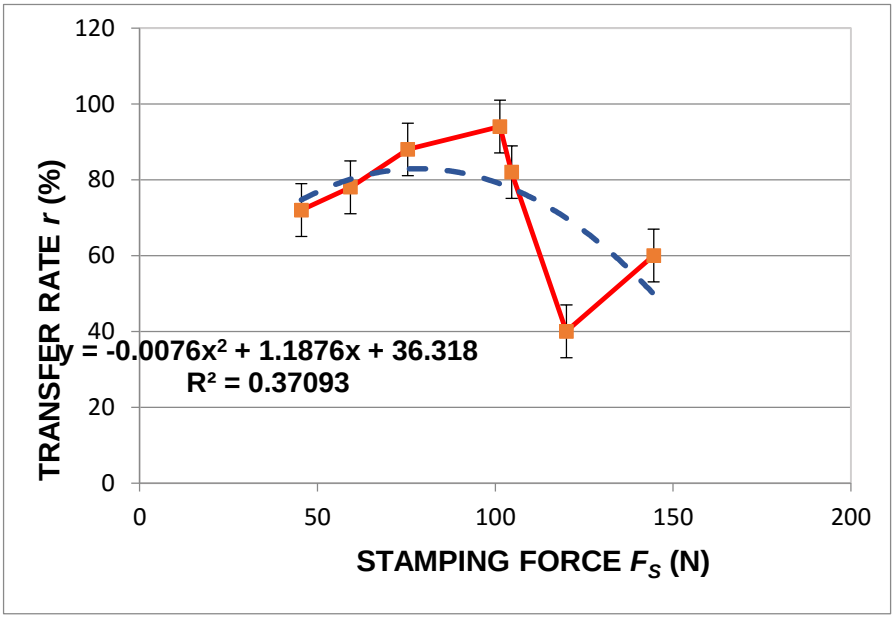

(b)

Figure 17: (a) Test samples with varied applied force for transfer characterization study. (b) Transfer rate vs. stamping force plot for transfer of toner particles

Transferring tests were also conducted by applying a stamping force varied from 27 N to 158 N on resin surfaces that were cured by a curing time of 7 seconds. Figure 17 (a) shows the actual test cases with varied applied transfer force and the transfer rates are plotted in Figure 17 (b). It is found that the transfer rate increases almost linearly with stamping forces in the early range, i.e. from 40 N to 100N. After the transfer rate approaches this maximum value, the increasing rate gets smaller.

3.4. Particle Deposition Accuracy Analysis

During the transfer process it is very important to carefully consider the transferring deposition method's accuracy, as some of the required parts require outstanding surface finish as well as good tolerance. The moving down velocity of the z-stage and velocity of the resin flow could affect the transfer accuracy of the desired dispersion pattern thus making it mandatory to conduct initial deposition analysis. In this section, we have analyzed the test cases under different velocities of the Z-stage (the motor which drives the primary platform up and down) and accordingly drawn conclusions. The results have been shown in Table 3 below. We varied the rate and quantity of toner particles transferred onto the built liquid resin model (yellow) to check how well the particles adhered to the liquid resin surface when we move the built model in the resin tank using the Z-stage and vary the speed of stage every time. Here, the toner particle pattern was transferred from the EDU to SL apparatus, and deposited on to the top layer of a freshly built liquid resin model. For this study, the part with pattern was taken down by the z-stage with different velocities inside the liquid resin tank, keeping the part for a good 3 seconds and then taken outside the tank with the same speed of the stage as earlier. As seen in Table 1, the right two columns show the picture of the adhesion of the toner particles to the liquid resin surface before and after the part model enters the liquid resin tank with controlled z-stage velocity. Thus, we can thus successfully conclude that the change in velocity of the z-stage does not affect the particle deposition pattern and the toner particles stay intact to the top cured resin surface. Also the liquid photopolymer with particle deposition pattern provides exceptional surface finish as well as good tolerance. Figure 18 shows the plot of the transfer rate accuracy vs the z-stage velocity.

TEST CASE NO.	VELOCITY OF THE Z-STAGE MOTOR	VELOCITY OF THE Z-STAGE MOTOR (in mm/s)	PICTURE OF THE BUILT MODEL WITH TRANSFER STAMP	PICTURE OF THE BUILT MODEL AFTER IMMERSING IN LIQUID RESIN
1	5000	1.67		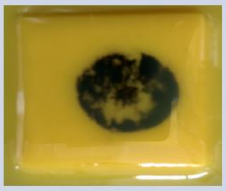
2	12000	4.008		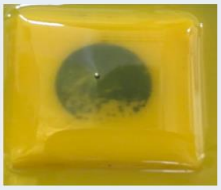
3	19000	6.346		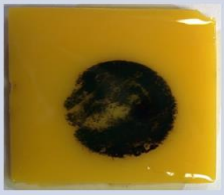
4	26000	8.684		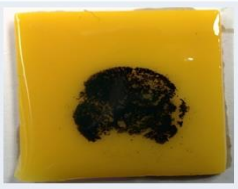
5	33000	11.022		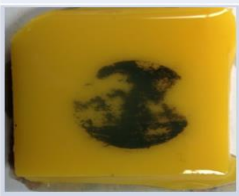
6	40000	13.36	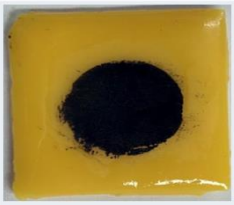	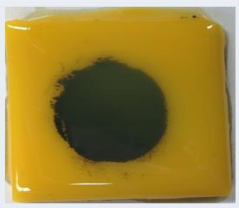

Table 1: Transfer rate deposition accuracy for parts at different z-stage velocity

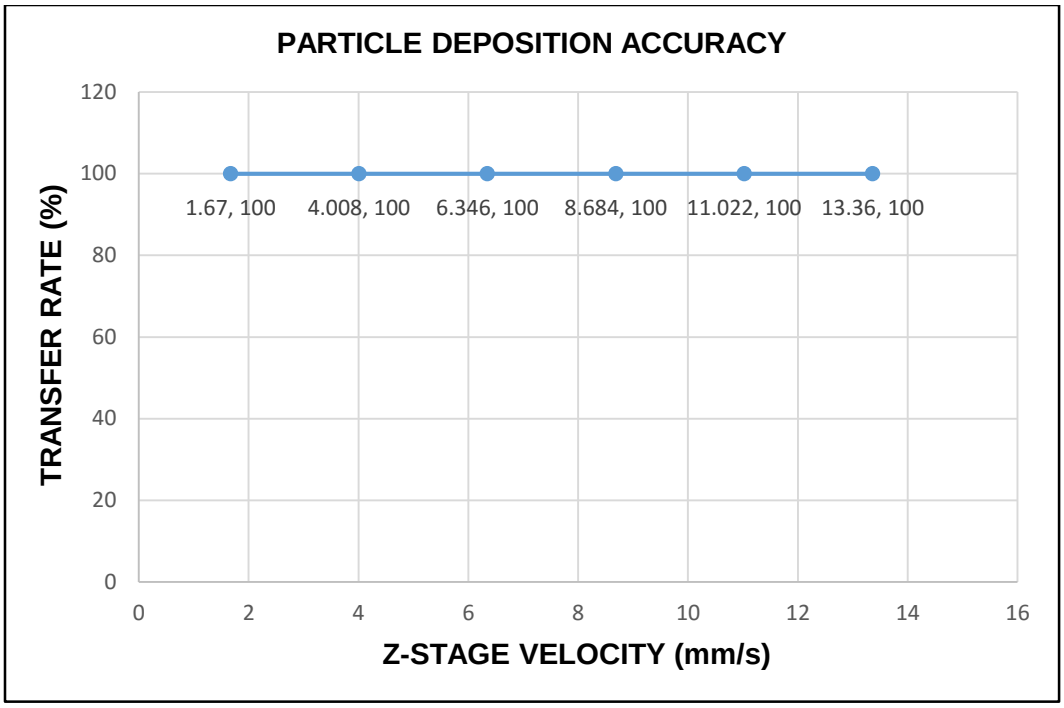

Figure 18: Deposition accuracy analysis plot showing the independence of particle dispersion pattern on z-stage velocity

3.5. Polymer-Particle Curing

3.5.1. Theoretical Photo-Curing Model

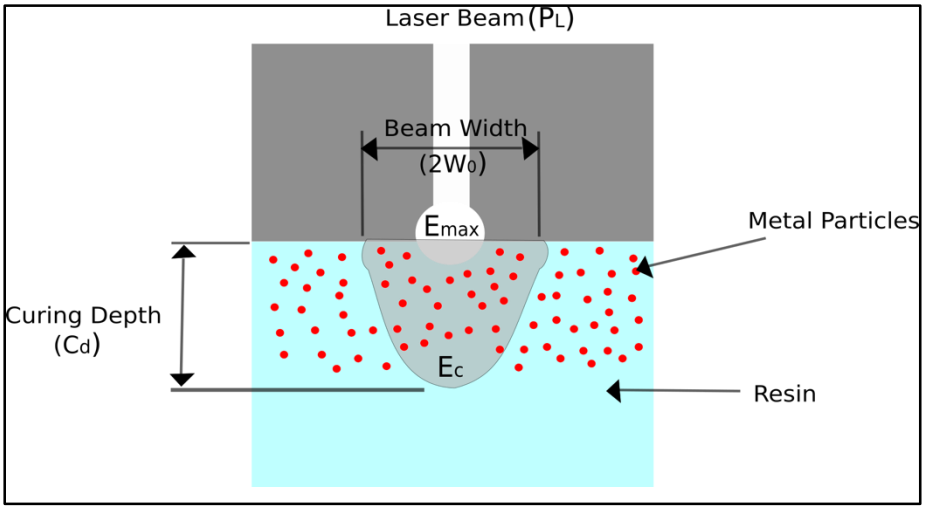

Figure 19: Schematic representation of the photo curing of the polymer-particle composite surface

Tremendous work has been done on projection based SL process. However, most of the work is based on pure photo polymer. Until now, little attention is drawn on composite fabrication. The main challenge is related to the different curing process between the pure resin and the composite slurry. For the pure resin, the curing process follows the Beer-Lambert law of absorption, which is formulated as the working curve [57]:

$$C_d = D_p \ln(E|E_c) \tag{14}$$

Where C_d is the curing depth, D_p, E and E_c are resin parameters known as the penetration depth of the resin, which is defined as $D_p = 1/(2.3\varepsilon[I])$ (where ε is the molar extinction coefficient of the initiator, $[I]$ is the initiator concentration), the exposure dose on the resin surface and critical exposure energy of the resin respectively. Critical exposure is the exposure corresponding to the energy, below which the polymerization does not happen [58].

In PES, we have a composite slurry that is composed of monomers, photo initiators and particles. The photo polymer is functioned as a binder that binds the particles together known as green part. When the light travels through the high concentrated composite slurry, it is dispersed by the particles and its propagation direction will be changed. Thus, the light is absorbed by the particle as well as curable resin. The working curve for traditional resin is limited by absorption. A new relation is used to describe the effect of scattering on curing depth, which is given as [59, 60]:

$$C_d = \frac{2d}{3Q\phi} \ln\left(\frac{E}{E_c}\right) \tag{15}$$

$$Q = \left(\frac{\Delta n}{n_0}\right)^2 \left(\frac{d}{\lambda}\right)^2 \tag{16}$$

Where d is the mean diameter of particles, ϕ is the volume fraction of the particle in the slurry, n_o is the refractive index of the resin, ∇n is the refractive indices difference between the

particle and the solution and λ is the light wavelength. As can be seen from this equation, the curing depth is predominantly controlled by the square of the refractive index difference between the particles and the polymer. Thus the study of the curing mechanics of the composite slurry is intricate and complicated than the traditional polymer based stereolithography process.

Now for a fixed kind of a particle, the light wavelength (λ), the mean diameter of particles (d) refractive indices difference between the particle and the solution (∇n) and the refractive index of the resin (n_o) remain constant i.e. Q is constant. Also in our case we consider weight fraction of the particle in the slurry as ϕ, which changes as we vary the amount of particles in the slurry. Thus Equation (15) reduces to:

$$C_d = \frac{K_1}{\emptyset} \left(\frac{lnt}{lnT_c}\right) \tag{17}$$

We can further write equation (17) as follows;

$$C_d = K_1 lnt\, \gamma - K_1 K_2 \gamma \tag{18}$$

where $K_1 = \frac{2d}{3Q}$,

$K_2 = \ln(T_c)$, and

$$\gamma = \frac{1}{\emptyset}$$

Thus equation (18) is the derived theoretical curing model for the curing mechanics of the particle-polymer slurry for this research work.

3.5.2. Experimental Photo-Curing Model

The theoretical curing depth model discussed is a basic model describing the relationship between the curing depth (C_d) and the photo-curing time (which governs the light intensity and thus the exposure energy, *E*). Whereas the desired physical model is a composite with solid particles deposited in the liquid photo curable resin. Thus the curing depth model considered for the PES process should also include the particle to photo curable resin weight ratio. We conducted some set of experiments for calculating the 'Dp' and 'tc' values for the photo-curable resin model (without the solid/metal particles)

S No.	Curing Time, t (s)	ln(Curing Time)	Curing Depth, C_d (mm) Experimental Readings				Average C_d (mm)
			1	2	3	4	
1	10	2.3025	0.23	0.22	0.24	0.25	0.235
2	12	2.4849	0.28	0.27	0.26	0.29	0.275
3	14	2.6390	0.3	0.32	0.31	0.32	0.312
4	16	2.77258	0.33	0.34	0.32	0.34	0.332
5	18	2.89037	0.35	0.36	0.37	0.38	0.365

Table 2: Experimental readings of curing depth against different curing times

The experimental readings as shown in Table 2 were further used to draw a plot depicting the relationship between curing depth and logarithmic of curing time, which can be further used to find out the unknown parameters like 'D_p' and 'T_c'.

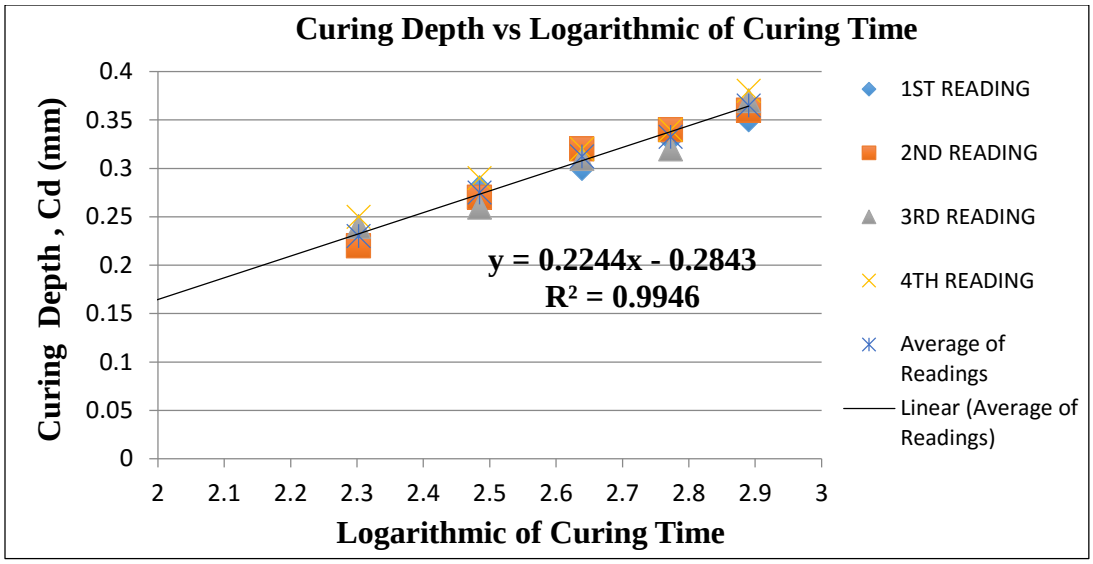

Figure 20: Plot of curing depth vs logarithmic of curing time validating the theoretical curing model

With the help of the experimental readings taken (as shown in Table 1) we calculated the depth of penetration of laser into resin/polymer until a reduction in irradiance of '$1/e$' is reached, Dp = 0.2244 mm & critical curing time, T_c = 3.55s by validating the theoretical curing depth model. The plot of curing depth vs logarithmic of curing depth is shown in Figure 20.

Now from the proposed new curing model, we consider the weight ratio of the particle to the resin by fitting a surface to the experimental model generated from the experimental readings. Based on the experimental readings collected for different curing times and weight ratios we predict a 3D model defining the relationship between the curing depth, weight ratio and the logarithmic of curing time (the exposure energy is directly controlled by the curing time). Figure 21 and Figure 22 show the plot of curing depth vs curing time and curing depth vs weight ratio respectively.

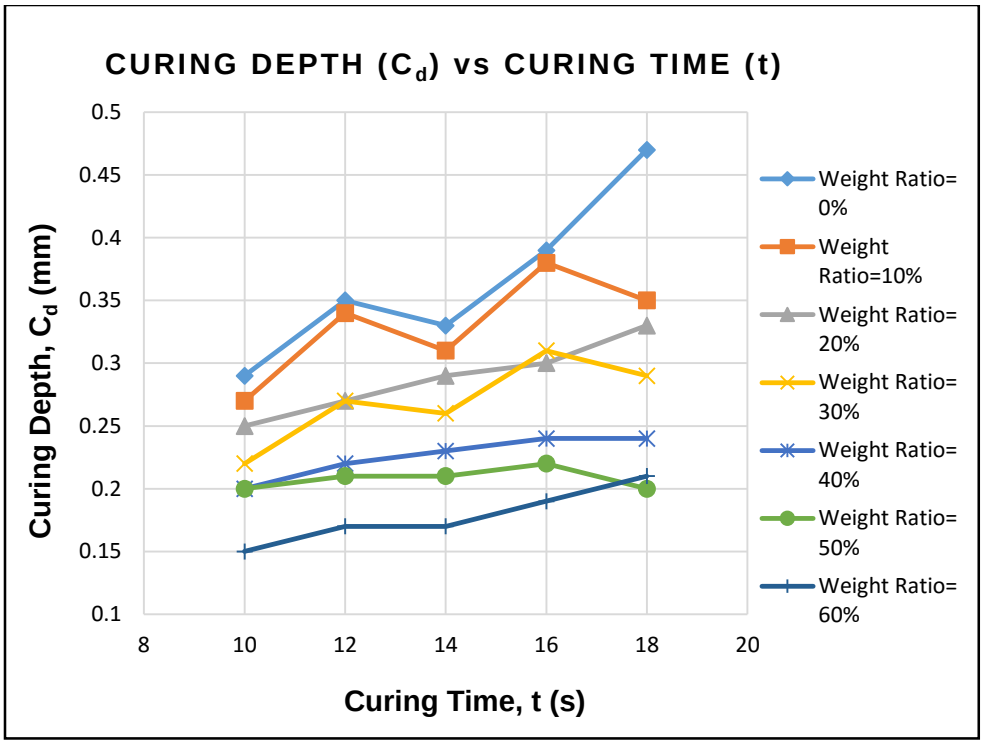

Figure 21: Plot of curing depth (in mm) vs curing time (in s)

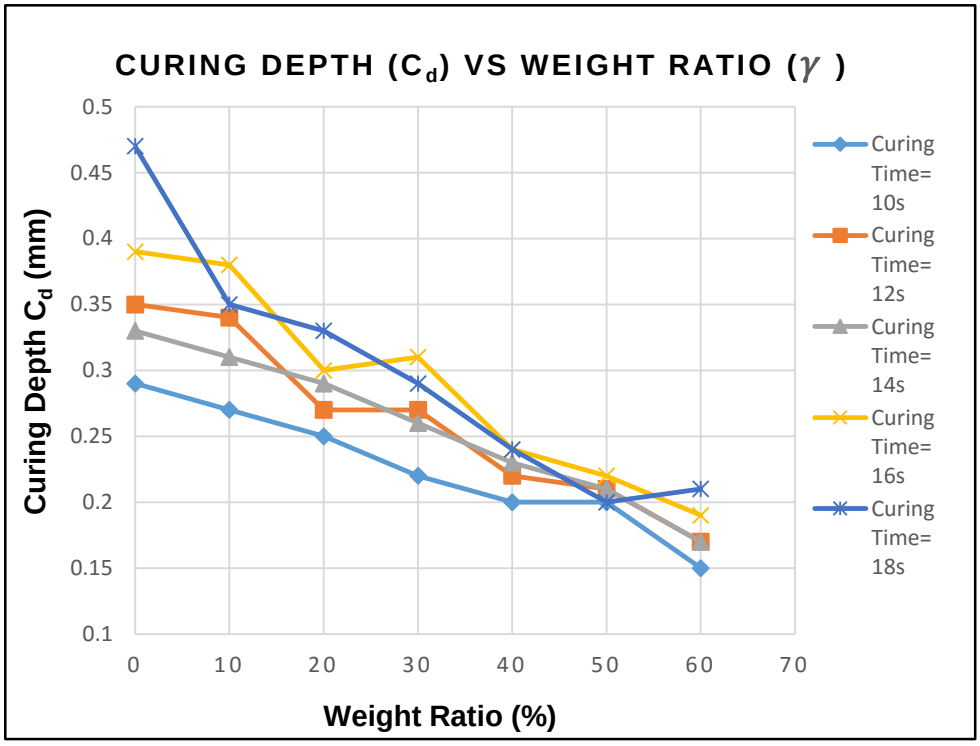

Figure 22: Plot of curing depth (in mm) vs weight ratio (%)

Now using the curve-fitting tool in Matlab R2015a software, we propose a 3D surface that gives the closest fit to all the data points generated in the experiments, and thus we will get the experimental curing model. Figure 23 (a) shows the 3D surface fit plot of the results of the curve-fitting tool. The surface shown in Figure 23 (a) is a surface model with polynomial equation with SSE and R^2 values of 0.02492 and 0.7447 respectively. Figure 23 (b) and (c) give the 2D plot of the curing depth vs ln(t)*γ and curing depth vs weight ratio (γ) respectively.

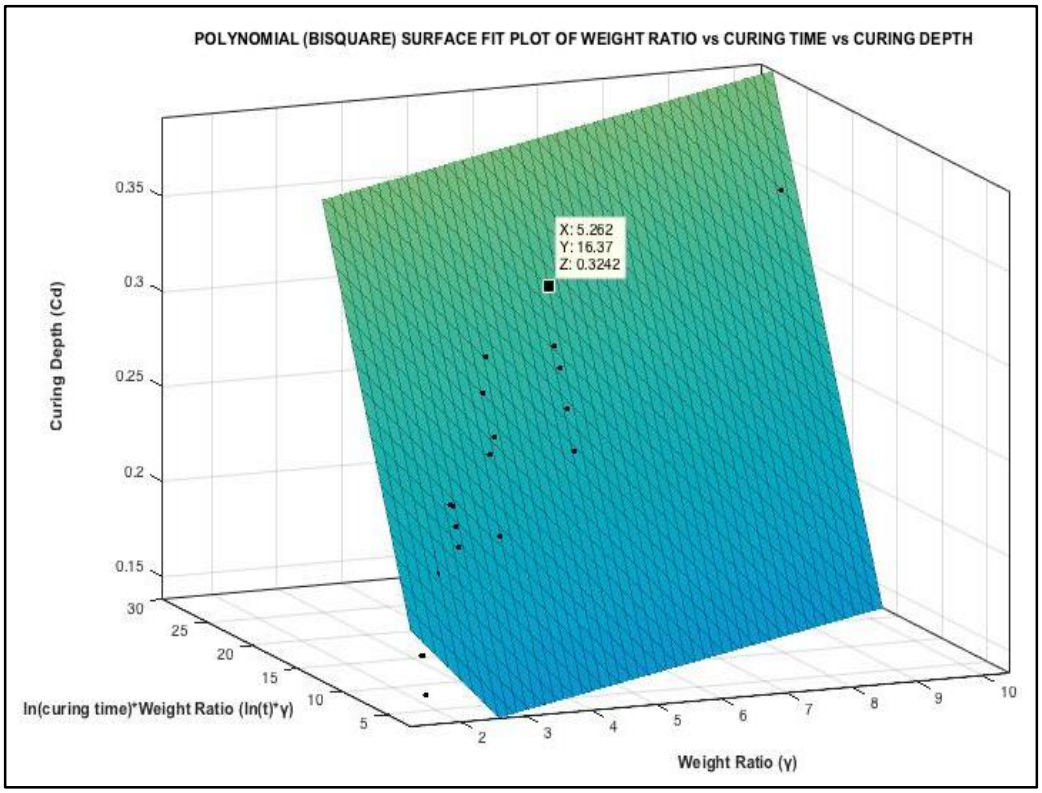

(a)

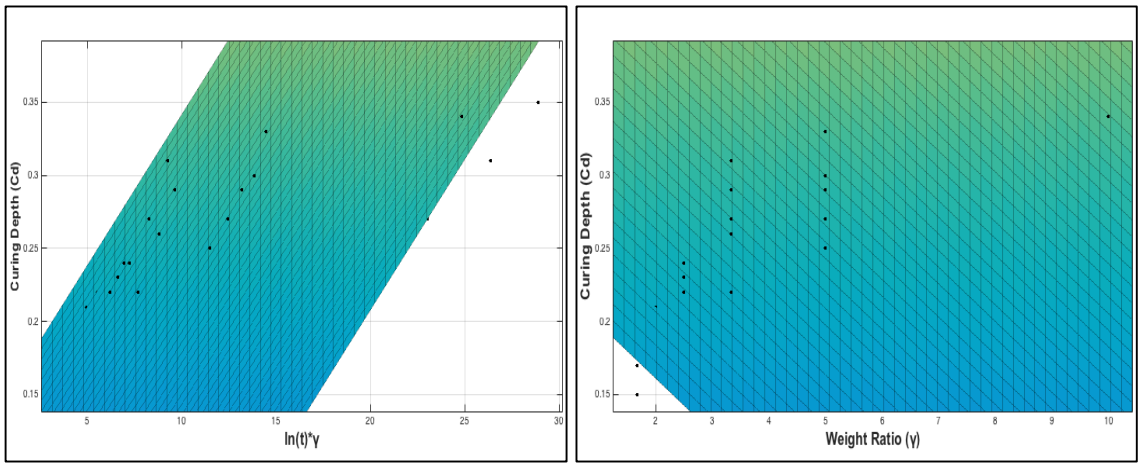

(b) **(c)**

Figure 23: Result of the curve fitting tool in Matlab R2015a (a) 3D surface fit plot of curing time, weight ratio and product of curing time& weight ratio (b) Y-Z view of the 3D plot, and (b) X-Z plot of the 3D plot

RESULTS OF THE POLYNOMIAL SURFACE FIT PLOT	
Linear Ploy11 Model	**Goodness of Fit**
f (x, y) = p00 + p10*x + p01*y where x is normalized by mean 4.083 and std 2.909 and where y is normalized by mean 10.69 and std 7.689 Coefficients (with 95% confidence bounds): p00 = 0.2508 (0.2395, 0.2622) p10 = -0.1079 (-0.1924, -0.02336) p01 = 0.1585 (0.07397, 0.243)	**SSE:** 0.02492 **R-square:** 0.7447 **Adjusted R-square:** 0.7258 **RMSE:** 0.03038

Table 3: Results of the surface fit plots deduced from curve fitting tool in Matlab R2015a

Thus the experimental model thus deduced from Figure 16 is: -

$$C_d = 0.1585 \ln(t)\, \gamma - 0.1079\ \gamma + 0.2508 \quad (19)$$

In Equation 19, the representation is as follows: -

γ = Weight Ratio (weight of polymer to weight of particles in gms),

C_d = Curing Depth (mm),

t = Curing Time (s)

3.6. Summary

This chapter introduces the particle deposition and transfer methods. The mechanics of electrostatic particle deposition is explained in detail. The parameters to be considered while the deposition process are investigated and analyzed. Next, the mechanism of transferring the particles from the electrostatic deposition to the SL unit is investigated. Different transfer approaches were considered, like liquid bridge approach and elastomeric stamping approach for this process. The stamping approach was preferred over the other approach because of its ease of use and higher transfer rate. A theoretical polymer-particle curing model was predicted and an experimental model was generated to verify the theoretical model successfully. Next, transfer process characterization from the collection film and PDMS film is inspected and the results for same are presented. Finally, the accuracy of the transfer process and the effect of different actuator is studied.

CHAPTER 4. EXPERIMENTAL RESULTS

[Parts of the content in this chapter is composed of previous work: Yayue Pan, Abhishek Patil, Ping Guo, Chi Zhou. "*A Novel Projection based Electro-Stereolithography (PES) Process for Production of 3D Polymer-particle Composite Objects*", Accepted and Forthcoming in Rapid Prototyping Journal, DOI: 10.1108/RPJ-02-2016-0030.]

Further to validate the feasibility of this novel Additive Manufacturing process we printed a few test cases using a composite polymer (EnvisonTEC Perfactory LS600M). Also the test particles used for this introductory study are the toner particles used in a HP LaserJet P1102w printer. We tried various dispersion patterns for composite printing using the polymer and the toner particles. These patterns were examined to evaluate the performance of the proposed process.

4.1. Test of photo-curing components

To make sure the proposed PES process and developed prototype system had no issues in the photo-curing part, two sample test cases were conducted. The manufacturing capability of the parts fabricated with pure resin was verified by first fabricating a spur gear and then a cube array. The photo-curing area is set at 135.80×103.124 mm.

The fabricated model of gear constitutes 122 layers in total, including 3 base layers with each layer thickness corresponding to 152.3 μm. Initial exposure time for the base layer was 150 seconds (2.5 minutes), whereas for the subsequent layer it was 15 seconds each. A sleeping time of 3 seconds is introduced when the stage goes down inside the resin tank to provide enough time to uniformly cover the top layer of the part with fresh resin. The entire building process was completed in 47 minutes, which also includes a total settling time of 21 seconds per layer (includes the projection time, sleep time and z-stage motion time). Since a top-down projection has been adopted, after each layer the platform travels down a certain distance (~2.5mm) and then while

retracting it adds one layer of liquid on its top. The gear design and fabricated parts are shown in Figure 24 (a) and (b).

The second test case for photo-curing process validation is a cube array as shown Figure 24 (c) and (d). This model is sliced into 14 layers in total, 0 images in image set P and 14 images in image set L. A larger layer thickness of 203.2 μm is used for this test. The cube array as shown in the Figure 7 is 38×38 mm and has a thickness of 2.84 mm.

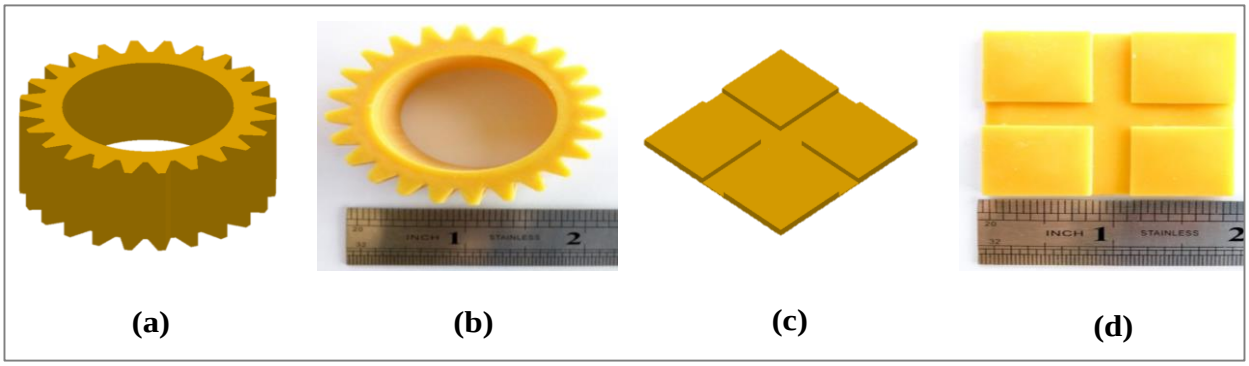

Figure 24: (a) CAD model of spur gear; (b) fabricated gear; (c) CAD model of cube array, (d) fabricated cube array

These two simple tests show that the mask image planning, light projection and liquid curing components worked properly and that the developed PES system is ready to receive particles for composite manufacturing.

4.2. Polymer + Particles Photo-Curing Test

Because our electrostatic unit was developed from a modified off-the-shelf 2D laser printer, the material-machine interactions in the electrostatic deposition process are not known yet. It should be noted that any particle (metals, polymers) which can be electrostatically transferred could be used as the particle materials. To eliminate the influence of unknown material properties on PES process performance, we use the original toner cartridge particles to

test the particle dropping and particle-resin curing components in the developed PES system in this thesis.

4.2.1. Test of Lateral Distribution of Particles with Designed Pattern

A cube array with particles forming the letters "UIC" on its top left surface was tested to validate the capability of PES technology in selectively distributing particles on a lateral plane.

Its CAD model and the fabricated part are shown in Figure 25. The model was sliced to 15 layers, generating 15 mask images in Image set L named "L_1, L_2 till L_15", and one mask image in Image set P named P_14. Image P_14 includes digital information of the "UIC" pattern for particle deposition and curing.

From layer #1 to layer #14, the part was built layer-by-layer using mask images in set L. After finishing the 14^{th} layer, image P_14 was the input image and the laser scanned the photoconductive surface to form a latent image on the photoconductor surface. The toner particles were deposited on the particle collection plate by electrostatic force. The elastomeric stamping approach was then used to transfer particles to the surface of the cured 14^{th} layer.

After this, the image P_14 was exposed directly on the particles to improve the bonding between particles and cured resin surface. The exposure time was about 20 seconds. After the 2nd curing step, the stage went inside the tank to coat a fresh resin layer for 15^{th} layer curing.

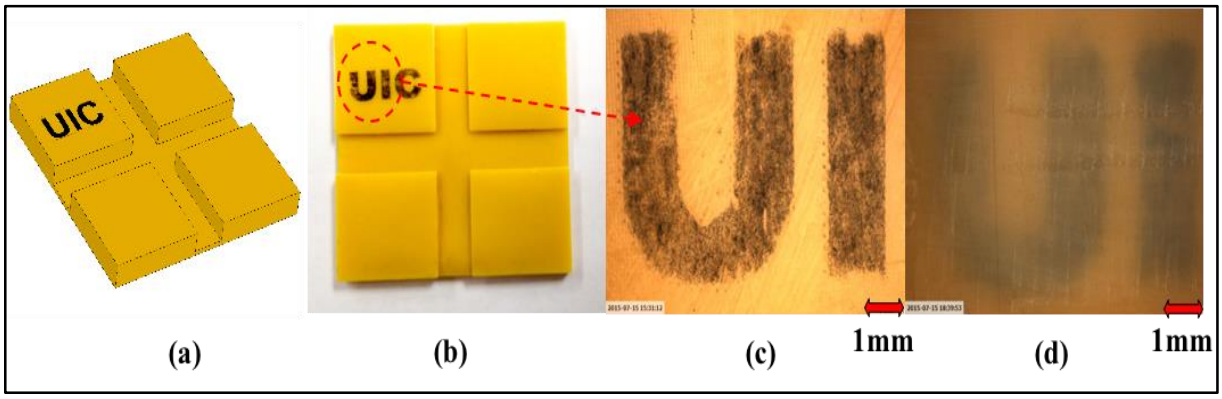

Figure 25: (a) CAD model, (b) fabricated cube array part without 15th layer, (c) microscopic images- top view of particles, and (d) microscopic image- top view of particles after 15th layer

One part was fabricated by stopping the building process at the 14th layer, so that the 15th layer of resin does not cover the particles. Figure 25 (b) shows the fabricated part without the 15th layer. Figure 25 (c) is the microscopic image of the blue-circled area in (b). It shows particles on the 14th layer. From Figure 25 (b) and (c), we can observe that the majority of particles have been transferred successfully from collection plate to resin surface. The "UIC" pattern formed by the electrostatic deposition process is retained pretty well after the transfer.

Another part is fabricated by completing the 15th layer. This way the UIC patterned particles are hidden below the top layer. Figure 9 (d) is the microscopic image of the same blue-circled area in this part, which has a layer of cured resin covering the particles. Because the top layer resin is only 203μm thick, the particles beneath are still visible, as shown in Figure 25 (d). Now to demonstrate the particles distribution pattern, two parts were fabricated which are discussed in the coming sections.

4.2.2. Test of Vertical Distribution of Particles with Designed Pattern

A cuboidal model was used to test the capability of PES technology in selectively distributing particles in the vertical direction with designed patterns. Toner particles (black color)

were imprinted on the 42nd and 46th layer of the 50 layers of the build part. The same manufacturing process with parameter settings as described in section 3 was used.

The CAD model and a fabricated part are shown in Figure 26 (a) and (b). The model is sliced to 50 layers. Image set L consists of 50 mask images named "L_1, L_2 till L_50", and image set P consists of two mask images named P_42 and P_46. These images deliver the digital information of the designed horizontal pattern for particle deposition and curing.

Figure 26 (c) and (d) are the microscopic images of the part. These figures show that particles are cured in designed layers. From the figures, the color distribution is very clear and even, such that we can distinctly differentiate between two particle layers from the actual and microscopic images.

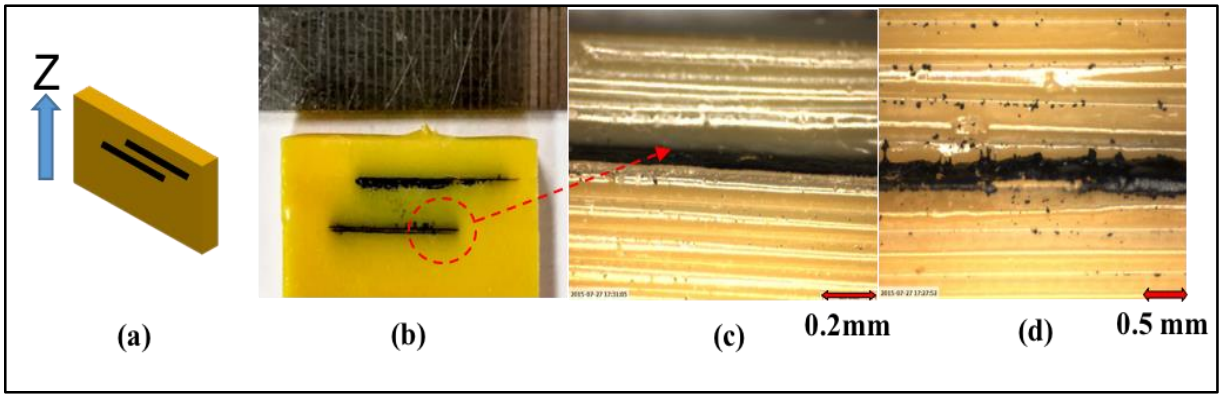

Figure 26: (a) CAD model, (b) top view of the fabricated model with toner particles in 42nd and 46th layer out of the 50 layers of the part, and (c-d) microscopic image of two areas in the fabricated part

4.2.3. An Electronic Circuit Testcase

A cuboidal model was again used to test the capability of PES technology in selectively distributing particles in the horizontal direction with designed patterns in the form of an electronic circuit. The toner particles (black color) were imprinted on the 20th layer of the build part. The same manufacturing process with parameter settings as described in section 3 was used.

The CAD model and the fabricated part are shown in Figure 27 (a) and (b) respectively. The model was sliced to 20 layers. The image set L consists of twenty mask images named "L_1, L_2 to L_20", and the image set P consists of one mask image named P_21. These images deliver digital information of the designed horizontal pattern for particle deposition and curing.

Figure 27 (c) and (d) are the microscopic images of the part. Figure 27 (c) shows the microscopic view of the electronic circuit pattern imprinted on the cured resin surface. It is clear that the particles are distributed with the designed circuit pattern. Figure 27 (d) shows the microscopic image after another layer of resin was cured over the particle circuit pattern.

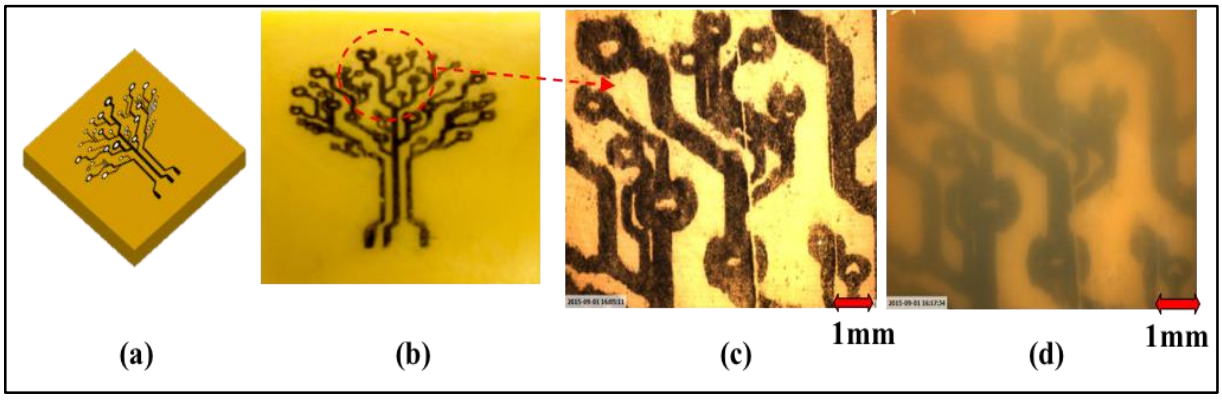

Figure 27:(a) CAD model, (b) top view of the fabricated model with toner particles on the 20th layer, (c) microscopic image-top view of the model of the transferred particles; and (d) microscopic image-top view of the model after 21st resin layer is cured

4.3. Study of Mechanical Properties

To investigate the influence of particle filling on mechanical properties of the printed part, we consider a dumbbell-shaped test specimen for determination of the tensile properties of the pure resin and particle-resin specimens. The standard dumbbell test specimens were tested under defined conditions of pretreatment, temperature, and testing machine speed [61]. The study of the tensile properties of polymer-particle specimen provides useful data for engineering design purposes.

The different mechanical properties, including maximum load, extension at break, Young's modulus, and tensile stress at break, were investigated for this thesis work. The tests were conducted according to the ASTM D638 standard test method for tensile properties of plastics [61]. The test specimens were generated from 3D CAD models to the dimensions specified in the relevant standards. Figure 28 shows the details of the tensile test specimen built as per the ASTM D638 Type 4 standard. Universal Testing System Instron 3365 (Capacity 5kN, Maximum speed 1000 mm/min) is used to conduct the tensile test for the specimens.

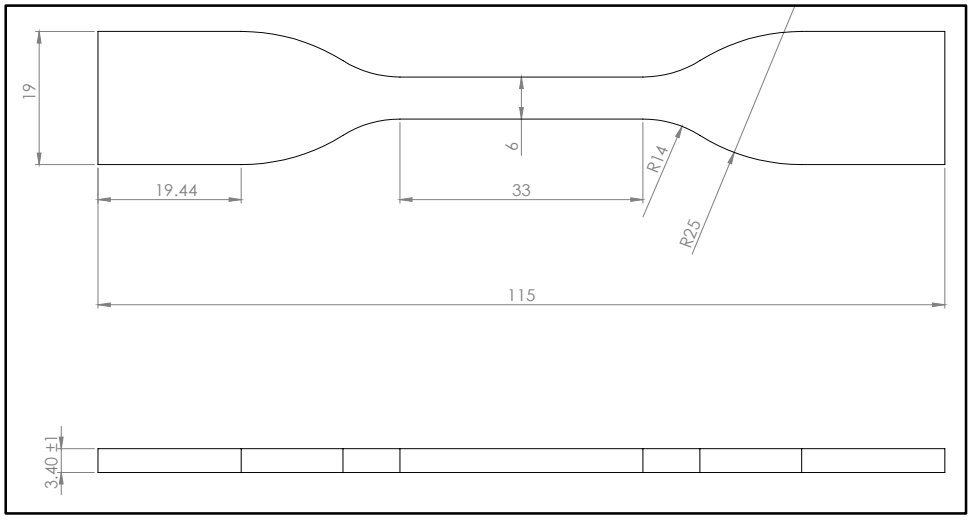

Figure 28: ASTM D638 Type 4 tensile test specimen **[62]**

Two different specimens were considered for the tensile test: test specimen without particles, and test specimen with particles (in every layer), as shown below in

Figure 29 (a) and (b) respectively. To determine and understand the mechanical properties of these 3-D printed parts and to investigate the variability in their properties, a user controlled printing setup and slicing parameters are used. Moreover, this study explores the relationship between particle deposition and filling patterns to maximum load, extension at break, tensile stress and modulus. The tests were carried using Perfactory LS600M resin and toner particles in the PES setup. Table 4 shows the printing parameters used.

Part Size (mm)	73.80 x 15.90 x 3.20 (l x b x h)
Layer Height (mm)	0.203
Infill (loading ratio of particles) (%)	0,16, 84,100

Table 4: Printing parameters for the test specimen

(a)

(b)

Figure 29: Test specimen built according to ASTM D638 Type 4 standard with different loading distribution of particles with polymer

In order to determine the mechanical properties of the test specimen, because of the size restrictions of the PES platform and uncontrollable specimen conditions, the actual print size of the test specimen deviated slightly from the ASTM D638 standard.

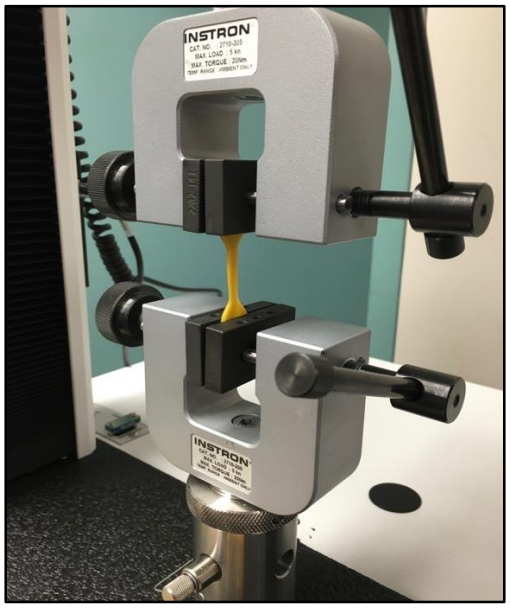

Figure 30: Digital picture of the test specimen in load frame of Instron 3365 machine

Results for the tensile test of specimens with particle loading ratio (0% & 100%) are given in Table 5.

S. No.	Part Type	Tensile Extension at Break (mm)	Maximum Load (N)	Tensile stress at Break (MPa)	Modulus (Young's) (MPa)
1	Part without Particles	1.86705	235.38454	18.46153	1178.80446
2	Part with Particles	2.85871	190.91426	9.76065	1051.13043

Table 5: Different mechanical properties of the printed test components

Figure 31 gives the plot of load vs. extension for these tested components. In the figure, the triangle points denote the point at which the part breaks. We can see that the specimen without particles (pure polymer) has higher maximum load compared to the part with particles in each layer throughout the surface of the specimen.

Whereas the part with particles (throughout the surface) has higher tensile extension at break than the test specimen without particles. In addition, it is interesting to observe that the part without particles breaks at maximum load whereas the part with particles breaks at a load lower than the maximum load. Referring to Table 5, we can also see that the Young's modulus is slightly higher for the specimen without particles indicating that it is still slightly more rigid than the specimen with particles

Strength is defined as the maximum stress (force/ unit cross sectional area) a material can withstand without rupture. Table 5 also shows that the part without particle has higher tensile stress at break whereas the part with particles throughout the surface has larger extension at break (almost 1mm more).

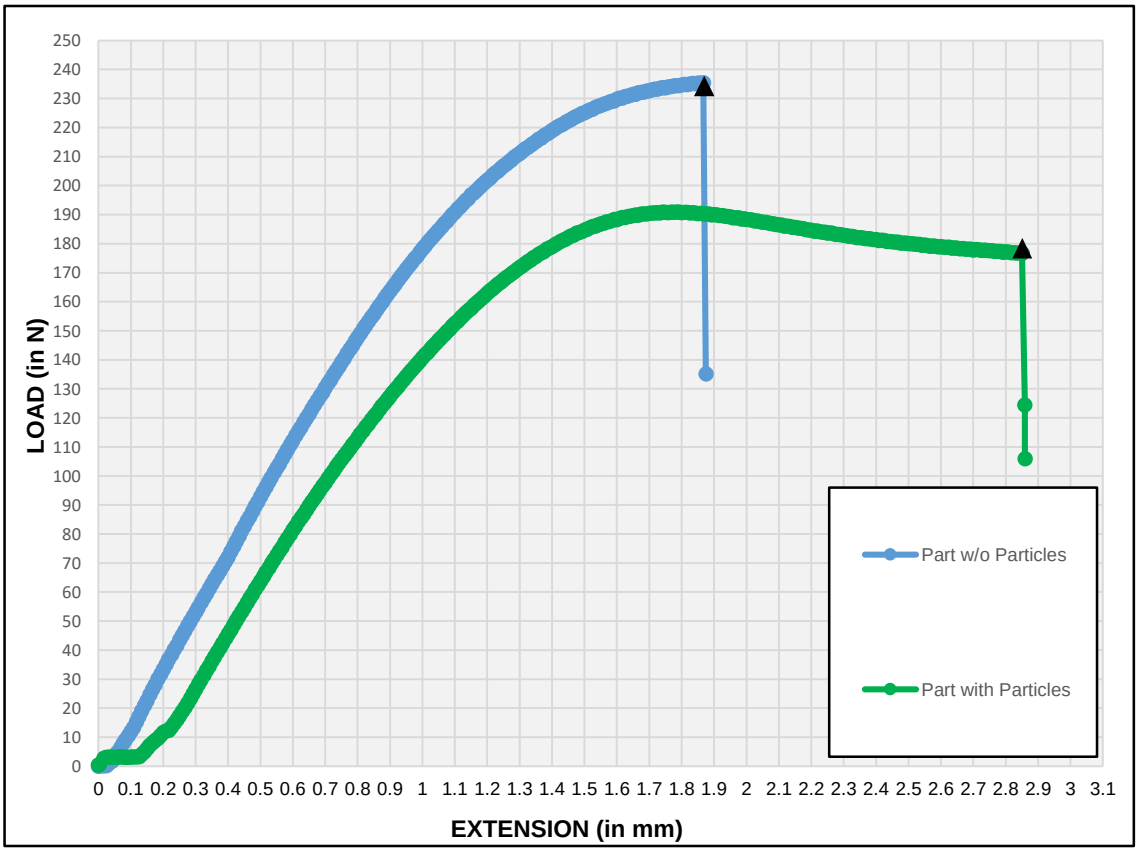

Figure 31: Load vs. extension plot of the two printed parts, one without particles and other with particles in every layer

Thus by analyzing the mechanical properties of these two specimens we can conclude that the specimen with particles has more tensile strength at break and slightly higher rigidity, while the specimen with particles has higher tensile extension at break but it loses its rigidity because of the introduction of the particles.

CHAPTER 5. CONCLUSION AND FUTURE WORK

[Parts of the content in this chapter is composed of previous work: Yayue Pan, Abhishek Patil, Ping Guo, Chi Zhou. "*A Novel Projection based Electro-Stereolithography (PES) Process for Production of 3D Polymer-particle Composite Objects"*, Accepted and Forthcoming in Rapid Prototyping Journal, DOI: 10.1108/RPJ-02-2016-0030.]

A novel additive manufacturing technology, Projection Electro-Stereolithography(PES), is developed in this thesis for polymer- particle composite printing. The proposed process uses electrostatic deposition approach to collect particles in a plate, and then uses stamping method to transfer particles to resin surface, hence is able to distribute particles into photopolymer layer by layer, with programmed patterns. Compared to existing multi-material 3D printing approach, which usually blend particles with liquid resin evenly first and then use the paste as raw material, PES has a unique advantage in local control of particle dispersions, addressing the historical challenge in polymer-particle composite fabrication. This unique characteristic could open a new avenue for advanced composite materials design and additive manufacturing functional products.

Feasibility and challenges in implementing this new technology are discussed in this thesis. First, collection of one layer of particles each time avoids the historical research problems in extending 2D electrophotography technique into 3D printing. Secondly, transferring of particles with well-kept patterns is investigated. Effects of collection plate materials, stamping force and curing time on transferring results are characterized. Accordingly, a proof-of-concept test bed has been developed. Case studies verified the capability of this new process on building composites with programmable particle filling patterns.

As a novel manufacturing technology, considerable work remains to mature the process and the related prototype system to overcome potential challenges and improve its performance. Some on-going investigations in our group include:

- Testing other particles for electrostatic depositing and transferring.

- Investigating other approaches for improving the bonding between particles and cured resin, like thermal fusing.

REFERENCES

1) Wong, K.V. and A. Hernandez, *A review of additive manufacturing.* ISRN Mechanical Engineering, 2012. **2012**.

2) Ha, Y.M., J.W. Choi, and S.H. Lee, *Mass production of 3-D microstructures using projection microstereolithography.* Journal of mechanical science and technology, 2008. **22**(3): p. 514-521.

3) Pan, Y.Y., C. Zhou, and Y. Chen, *A Fast Mask Projection Stereolithography Process for Fabricating Digital Models in Minutes.* Journal of Manufacturing Science and Engineering-Transactions of the Asme, 2012. **134**(5).

4) Pan, Y. and Y. Chen, *Smooth Surface Fabrication based on Controlled Meniscus and Cure Depth in Micro-Stereolithography.* 2015.

5) Pan, Y., Zhao, X., Zhou, C. and Chen, Y., 2012. Smooth surface fabrication in mask projection based stereolithography. *Journal of Manufacturing Processes*, *14*(4), pp.460-470.

6) Sun, C., N. Fang, D. M. Wu, and X. Zhang. "Projection micro-stereolithography using digital micro-mirror dynamic mask." *Sensors and Actuators A: Physical* 121, no. 1 (2005): 113-120.

7) Pan, Y., Zhou, C., Chen, Y. and Partanen, J., 2014. Multitool and multi-axis computer numerically controlled accumulation for fabricating conformal features on curved surfaces. *Journal of Manufacturing Science and Engineering*, *136*(3), p.031007.

8) Turner, B.N., R. Strong, and S.A. Gold, *A review of melt extrusion additive manufacturing processes: I. Process design and modeling.* Rapid Prototyping Journal, 2014. **20**(3): p. 192-204.

9) Zhao, X., Pan, Y., Zhou, C., Chen, Y. and Wang, C.C., 2013. An integrated CNC accumulation system for automatic building-around-inserts. *Journal of Manufacturing Processes*, *15*(4), pp.432-443.

10) Huang, S.H., Liu, P., Mokasdar, A. and Hou, L., 2013. Additive manufacturing and its societal impact: a literature review. *The International Journal of Advanced Manufacturing Technology*, *67*(5-8), pp.1191-1203.

11) Berman, B., *3-D printing: The new industrial revolution.* Business Horizons, 2012. **55**(2): p. 155-162.

12) Materials, P.D. [Cited 2015 7/15]; Available at: http://www.stratasys.com/materials/polyjet/digital-materials.

13) Khalil, S., Nam, J. and Sun, W., 2005. Multi-nozzle deposition for construction of 3D biopolymer tissue scaffolds. *Rapid Prototyping Journal*, *11*(1), pp.9-17.

14) Zhou, C., Chen, Y., Yang, Z.G. and Khoshnevis, B., 2011. Development of Multi-Material Mask-Image-Projection-Based Stereolithography for the Fabrication of Digital Materials. In *Annual Solid Freeform Fabrication Symposium, Austin, TX*.

15) Liew, C.L., Leong, K.F., Chua, C.K. and Du, Z., 2002. Dual material rapid prototyping techniques for the development of biomedical devices. Part 2: secondary powder deposition. *The International Journal of Advanced Manufacturing Technology*, *19*(9), pp.679-687.

16) Liew, C.L., Leong, K.F., Chua, C.K. and Du, Z., 2001. Dual material rapid prototyping techniques for the development of biomedical devices. Part 1: Space creation. *The International Journal of Advanced Manufacturing Technology*, *18*(10), pp.717-723.

17) Jackson, B., K. Wood, and J. Beaman, *Discrete multi-material selective laser sintering (M 2 SLS): development for an application in complex sand casting core arrays.* Proc Solid Freeform Fabr, 2000. **2000**: p. 176-182.

18) Santosa, J., D. Jing, and S. Das, *Experimental and numerical study on the flow of fine powders from small-scale hoppers applied to SLS multi-material deposition–part I.* Ann Arbor, 2002. **1001**: p. 48109-2125.

19) Bartolo, P. and J. Gaspar, *Metal filled resin for stereolithography metal part.* CIRP Annals-Manufacturing Technology, 2008. **57**(1): p. 235-238.

20) Kumar, S. and J.-P. Kruth, *Composites by rapid prototyping technology.* Materials & Design, 2010. **31**(2): p. 850-856.

21) Wurm, G., Tomancok, B., Holl, K. and Trenkler, J., 2004. Prospective study on cranioplasty with individual carbon fiber reinforced polymere (CFRP) implants produced by means of stereolithography. *Surgical neurology*, *62*(6), pp.510-521.

22) Shahinpoor, Mohsen, Y. Bar-Cohen, J. O. Simpson, and J. Smith. "Ionic polymer-metal composites (IPMCs) as biomimetic sensors, actuators and artificial muscles-a review." *Smart materials and structures* 7, no. 6 (1998): R15.

23) Shahinpoor, Mohsen. "Ionic polymer–conductor composites as biomimetic sensors, robotic actuators and artificial muscles—a review." *Electrochimica Acta* 48, no. 14 (2003): 2343-2353.

24) Shahinpoor, Mohsen, and Kwang J. Kim. "Ionic polymer–metal composites: IV. Industrial and medical applications." *Smart materials and structures* 14, no. 1 (2004): 197.

25) Shahinpoor, Mohsen, Kwang J. Kim, and Mehran Mojarrad. *Artificial muscles: applications of advanced polymeric nanocomposites*. CRC Press, 2007.

26) Srivastava, Samanvaya, Jennifer L. Schaefer, Zichao Yang, Zhengyuan Tu, and Lynden A. Archer. "25th anniversary article: polymer–particle composites: phase stability and applications in electrochemical energy storage." *Advanced Materials* 26, no. 2 (2014): 201-234.

27) Jones, J., Wimpenny, D., Gibbons, G. and Sutcliffe, C., 2010, January. Additive manufacturing by electrophotography: challenges and successes. In*NIP & Digital Fabrication Conference* (Vol. 2010, No. 2, pp. 549-553). Society for Imaging Science and Technology.

28) Kumar, A.V., A. Dutta, and J.E. Fay, *Electrophotographic printing of part and binder powders.* Rapid Prototyping Journal, 2004. **10**(1): p. 7-13.

29) Kumar, A.V., A. Dutta, and J.E. Fay. *Solid freeform fabrication by electrophotographic printing*. in *14th Solid Freeform Fabrication symposium*. 2003.

30) Kumar, A.V. and A. Dutta, *Investigation of an electrophotography based rapid prototyping technology.* Rapid Prototyping Journal, 2003. **9**(2): p. 95-103.

31) Cross, J., *Electrostatics: principles, problems and applications.* 1987.

32) Kumar, A.V. and A. Dutta, *Electrophotographic layered manufacturing.* Journal of manufacturing science and engineering, 2004. **126**(3): p. 571-576.

33) Das, Ajay Kumar. "An investigation on the printing of metal and polymer powders using electrophotographic solid freeform fabrication." PhD diss., University of Florida, 2004.

34) Cormier, Denis, James Taylor, Kittinan Unnanon, Parikshit Kulkarni, and Harvey West. "Experiments in layered electro-photographic printing." In *Proceedings of the SFF Symposium*, pp. 267-274. 2000.

35) Arciniegas, R., (2013), "Towards the Control of Electrophotographic-Based 3-Dimensional Printing: Image-Based Sensing and Modeling of Surface Defects." Doctoral Dissertation. Rochester Institute of Technology.

36) 3D Systems Multijet process [Accessed 2015 07/15]; Available at: http://www.3dsystems.com/resources/information-guides/multi-jet-printing/mjp

37) Stratasys PolyJet Technology [Accessed 2015 7/15]; Available at: http://www.stratasys.com/3d-printers/technologies/polyjet-technology

38) Stratasys 3D printed part [Accessed 2016 2/5]; Available at: http://www.stratasys.com/~/media/Image-Gallery/color_cm_and_rubber_headphones.jpg?bc=White&as=0&h=380&w=650

39) 3D Systems 3D printed part [Accessed 2016 2/5]; Available at: http://www.3dsystems.com/sites/www.3dsystems.com/files/styles/ddd_printer-gallery_xl/public/visijet-5500x-composite-clear_0.jpg

40) Lappo, K., B. Jackson, K. Wood, D. L. Bourell, and J. J. Beaman. "Discrete multiple material selective laser sintering (M2SLS): experimental study of part processing." In *Solid Freeform Fabrication Symposium*, pp. 109-19. 2003.

41) Lappo, K., K. Wood, D. Bourell, and J. J. Beaman. "Discrete multiple material selective laser sintering (M2SLS): nozzle design for powder delivery." In *SFF Symposium*. 2003.

42) Pan, Yayue, Chi Zhou, and Yong Chen. "Rapid manufacturing in minutes: the development of a mask projection stereolithography process for high-speed fabrication." In *ASME 2012 International Manufacturing Science and Engineering Conference collocated with the 40th North American Manufacturing Research Conference and in participation with the International Conference on Tribology Materials and Processing*, pp. 405-414. American Society of Mechanical Engineers, 2012.

43) LS600 ABS-Like 3D Printer Material Data Sheet [Accessed 2016 02/25]; Available at: http://envisiontec.com/envisiontec/wp-content/uploads/MK-MTS-LS600-V01-FN-EN.pdf

44) Das, Ajay Kumar. "An investigation on the printing of metal and polymer powders using electrophotographic solid freeform fabrication." PhD diss., University of Florida, 2004.

45) Rimai, D., D. Weiss, and D. Quesnel, *Particle adhesion and removal in electrophotography.* Journal of adhesion science and technology, 2003. **17**(7): p. 917-942.

46) Rimai, D.S., S.o.P. Adhesion, and A. Society, *Advances in particle adhesion:[selected papers from the Symposium on Particle Adhesion at the 17th annual meeting of the Adhesion Society, Orlando, Florida, USA, February 21-23, 1994]*. 1996: Gordon & Breach.

47) Johnson, K., K. Kendall, and A. Roberts. *Surface energy and the contact of elastic solids*. in *Proceedings of the Royal Society of London A: Mathematical, Physical and Engineering Sciences*. 1971. The Royal Society.

48) Rimai, D. and D.J. Quesnel, *Fundamentals of particle adhesion*. 2001: Global Press.

49) AL-Rubaiey, H., *Toner Transfer and Fusing in Electrophotography.* Graphic Arts in Finland, 2010. **39**: p. 1.

50) Benilov, E.S. and C.P. Cummins, *The stability of a static liquid column pulled out of an infinite pool.* Physics of Fluids, 2013. **25**(11).

51) Gao, S., Jin, L., Du, J. and Liu, H., 2011. The Liquid-Bridge with Large Gap in Micro Structural Systems. *Journal of Modern Physics*, *2*(05), p.404.

52) Knospe, C.R. and H. Haj-Hariri, *Capillary force actuators: Modeling, dynamics, and equilibria.* Mechatronics, 2012. **22**(3): p. 251-256.

53) Yang, L., Y. Tu, and H. Fang, *Modeling the rupture of a capillary liquid bridge between a sphere and plane.* Soft Matter, 2010. **6**(24): p. 6178-6182.

54) Bowden, N., S.R.J. Oliver, and G.M. Whitesides, *Mesoscale self-assembly: Capillary bonds and negative menisci.* Journal of Physical Chemistry B, 2000. **104**(12): p. 2714-2724.

55) Nosonovsky, M. and B. Bhushan, *Multiscale effects and capillary interactions in functional biomimetic surfaces for energy conversion and green engineering.* Philosophical Transactions of the Royal Society a-Mathematical Physical and Engineering Sciences, 2009. **367**(1893): p. 1511-1539.

56) Chen, H., T. Tang, and A. Amirfazli, *Liquid transfer mechanism between two surfaces and the role of contact angles.* Soft matter, 2014. **10**(15): p. 2503-2507.

57) F.P. Jacobs, “Rapid Prototyping and Manufacturing: Fundamentals of Stereolithography”, Society of Manufacturing Engineers, Dearborn, MI, 1992.

58) Zhang, X., X. N. Jiang, and C. Sun. "Micro-stereolithography of polymeric and ceramic microstructures." *Sensors and Actuators A: Physical* 77, no. 2 (1999): 149-156.

59) M.L. Griffith, J.W. Halloran, “Stereolithography of ceramics,” Proc. of 27th International SAMPE Technical Conference, Albuquerque, NM, USA, Oct 9–12 Vol. 27, pp. 970–979, 1995.

60) M.L. Griffith, J.W. Halloran, “Freeform fabrication of ceramics via stereolithography,” J. Am. Ceram. Soc. 2601–2608, 1996.

61) American Society for Testing and Materials (Filadelfia). "Standard Test Method for Tensile Properties of Plastics." ASTM, 1998.

62) Datapoint Labs ASTM D638 Type IV CAD drawing [Accessed 2016 03/10]; Available at: https://www.datapointlabs.com/Images/Specimens/ASTM_D638_TypeIV.pdf

APPENDIX

Dear Abhishek,

Thank you for your email.

Please allow me to introduce myself, my name is Chris Tutill and I am the Rights Executive here at Emerald.

In answer to your question, Emerald allows its authors to include a published version of their article/chapter within their printed written thesis/dissertation.

If your Institution requires you to deposit an electronic copy, upon official publication, Emerald allows its authors to place a non-Emerald branded version of your article/chapter within your current institution's website. By this we mean that while it can have all of the Editorial changes, it must be in a different format – i.e. different font, different layout, etc. and must not have any Emerald logos or branding. We also ask that you include the DOI of the article (Found in abstract/document info).

We request that the following statement appears on each page;

'This article is © Emerald Group Publishing and permission has been granted for this version to appear here (please insert the web address here). Emerald does not grant permission for this article to be further copied/distributed or hosted elsewhere without the express permission from Emerald Group Publishing Limited.'

If the article/chapter will not be published prior to your dissertation being printed, we would request that you state the article is 'forthcoming in RPJ …'.

If possible, we would request that the article is not deposited online prior to official publication by Emerald- if this is likely, please request an embargo period to ensure that Emerald has first publication.

For more information on what you can do as an Emerald author with your work, please see our Emerald author rights page: http://www.emeraldinsight.com/authors/writing/author_rights.htm

I hope the above has answered your question but should you require any further information, please don't hesitate to contact me.

Many thanks
&
Kind Regards,

Chris Tutill
Rights Assistant | Emerald Group Publishing Limited
Fax: +44 (0)1274 785200
CTutill@emeraldinsight.com| www.emeraldinsight.com

VITA

NAME	Abhishek Patil
EDUCATION	B.E., Mechanical Engineering, Symbiosis International University, Pune, India, 2014. M.S., Industrial Engineering, University of Illinois at Chicago, Chicago, Illinois, U.S., 2016.
PUBLICATIONS	Yayue Pan, Abhishek Patil, and Chi Zhou. "*A Novel Projection based Electro-Stereolithography (PES) Process for Composite Printing*." International Solid Freeform Fabrication Symposium, Austin, Texas, 2015, pp. 1-16. Yayue Pan, Abhishek Patil, Ping Guo, Chi Zhou. "*A Novel Projection based Electro-Stereolithography (PES) Process for Production of 3D Polymer-particle Composite Objects*". Accepted and Forthcoming in Rapid Prototyping Journal, DOI: 10.1108/RPJ-02-2016-0030